Chapter 1

An Overview on Quantum Cascade Lasers: Origins and Development

Raúl Pecharromán-Gallego

Additional information is available at the end of the chapter

http://dx.doi.org/10.5772/65003

Abstract

This chapter presents an introductory review on quantum cascade lasers (QCLs). An overview is prefaced, including a brief description of their beginnings and operating basics. Materials used, as well as growth methods, are also described. The possibility of developing GaN-based QCLs is also shown. Summarizing, the applications of these structures cover a broad range, including spectroscopy, free-space communication, as well as applications to near-space radar and chemical/biological detection. Furthermore, a number of state-of-the-art applications are described in different fields, and finally a brief assessment of the possibilities of volume production and the overall state of the art in QCLs research are elaborated.

Keywords: quantum cascade lasers, review, history, operation, fundamentals, materials, photoacoustic spectroscopy, sensors, trace-gas detection, plasma species, cavity ring-down spectroscopy

1. Introduction

Quantum cascade lasers (QCLs) are based on a fundamentally different principle to 'classic' semiconductor lasers, that is, they use only one type of charge carriers, electrons, using intersubband transitions, so they can be called unipolar lasers. QCLs were conceived in the early 1970s. First, Esaki and Tsu [1] fabricated the first one-dimensional periodic potential multilayer by periodically varying the composition during epitaxial growth (superlattice). Later, QCLs were proposed by Kazarinov and Suris [2] and finally first demonstrated at Bell Laboratories in 1994 by Faist et al. [3]. Using superlattices leads to both quantum confinement and tunnelling phenomena, the basic processes in QCLs operation.

A conventional laser diode generates light by a single photon that is generated from an electron interband transition; this means that a high-energy electron in the conduction band recombines with a hole in the valence band, being the energy of the photon determined by the band-gap energy of the material system used. However, QCLs do not use bulk semiconductor materials in their optically active region, but a periodic series of thin layers of varying material composition forming a superlattice, which leads to an electric potential that changes across the length of the device (one-dimensional multiple quantum well confinement), splitting the band-permitted energies into a number of discrete electronic subbands, making electrons cascade down a series of identical energy steps built into the material during crystal growth, and emitting a photon at every step, unlike diode lasers, which emit only one photon over the equivalent cycle. With an appropriate design of the thickness of these layers, population inversion is achieved between discrete conduction band-excited states in the coupled quantum wells by the control of tunnelling, making laser emission possible. Therefore, the position of energy levels is mainly determined by the thickness of the layers, rather than the material, and thus allowing tuning the emission wavelength of QCLs over a wide range in the same material system. Thus, one electron emits a photon during every intersubband transition within the quantum well (QW) in the superlattice, and then can tunnel into the next period of the structure where another electron can be emitted, leading QCLs to outperform diode lasers operating at the same wavelength by a factor even greater than 1000 in terms of power.

Classically, a QCL is made of a periodic repetition of active sections, which consist of tunnel-coupled quantum wells and injector, where a miniband is formed. As **Figure 1** shows [4], from the injector miniband the electrons are injected into the upper laser energy level (4) of the active section, where the laser transition takes place. Afterwards, the lower laser energy level (3) is emptied by longitudinal optical emissions (LO emissions) and the electrons enter the next step by tunnelling.

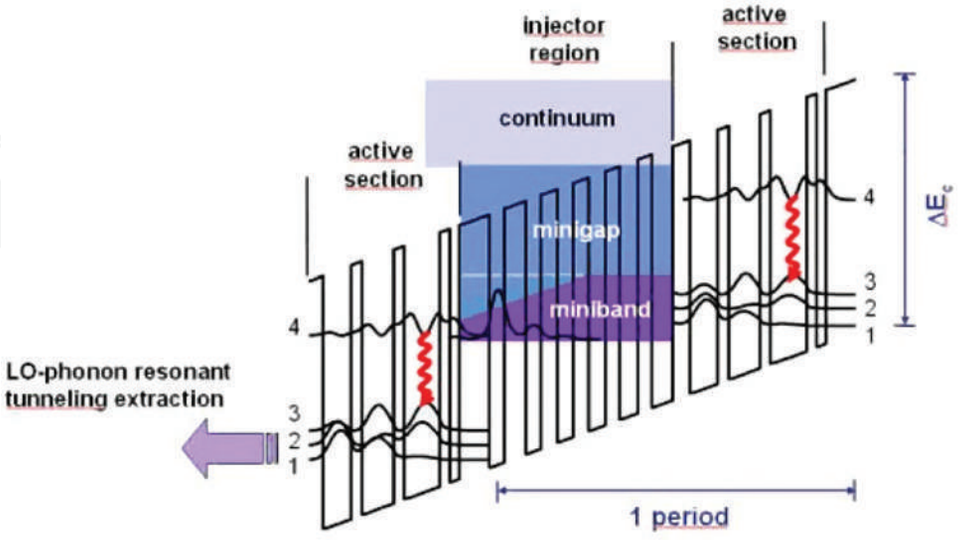

Figure 1. Typical conduction band structure of a QCL [4].

http://dx.doi.org/10.5772/65003

Combining materials in the active region, QCLs could be designed to emit at any wavelength over a wide range of the spectrum [5], as the emission wavelength is determined by quantum confinement. **Figure 2** shows a typical QCL in operation and some commercial examples. These structures are typically grown using either molecular beam epitaxy (MBE) or metal-organic chemical vapour deposition (MOCVD), being the most used growth mechanisms utilized to grow the alternated different semiconductor layers required for heterostructures fabrication on to a substrate. Ever since the first QCL was fabricated using InGaAs/InAlAs grown over InP substrate [1], other materials have been used in order to fabricate QCL structures, such as GaAs/AlGaAs, InGaAs/AlAsSb, InAs/AlSb, Si/SiGe and GaN-based materials, such as AlGaN/GaN and AlN/GaN.

Figure 2. Left: the invisible beam from a high-power quantum cascade laser lights a match in its path. The laser is 2.25 mm long and 17 μm wide, being placed in a cryostat at liquid-nitrogen temperature and emits an optical power in excess of 200 mW from each facet at a wavelength of 8.0 μm. Similar devices emit up to 600 mW at room temperature in pulsed mode. Right: front: mid-IR lasers (4–10 μm) for trace-gas analysis and IR molecular spectroscopy in the front; back: set-up examples.

First commercialized a decade later of their first demonstration [6], the key features of these lasers reside in the fact of their high optical power output and, on the other hand, their tuning range and room-temperature operation. Spectroscopy applications are related to gas detection and analysers (pollutants, components, etc.). Other practical uses include industrial control, plasma chemistry and detection, such as collision avoidance radar or poor visibility-driving condition aids. Finally, the 3 to 5μm atmospheric window would make QCLs perfect candidates for substitution of optical fibre in high-speed and free-space communications.

2. Fundamentals and operating principles

The main particularity in QCLs is the fact that instead of using bulk semiconductor materials in their optically active region, a periodic series of thin layers are used, that is, superlattices, consisting of a number of quantum well—barrier system equally spaced, introducing a multiple quantum well (MQW) leading to one-dimensional confinement allowing an electric potential variation (band splitting) that results in a number of discrete electronic subbands. In order to achieve the population inversion required for laser emission, it is necessary for a

proper thickness and composition layer design. These confined energy levels depend on the layer thickness, so the tunability of the emission within the same material relies, in principle, on thickness variation, although multiwavelength QCLs emit by means of different materials within the same structure and multiple resonators [7, 8].

In classical semiconductor laser diodes, electrons and holes recombine across the band gap, thus, generating one photon per e^--h^+ pair recombined. However, in QCLs this is not the case, as an electron in the conduction band within a QW emits one photon whenever it undergoes an intersubband transition, that is, thermalization into lower-energy levels, emitting one photon. This electron could tunnel into the next period of the structure, where the mentioned transition happens again emitting another photon. This phenomenon of a single electron emitting multiple photons as it passes through different periods of the structure is called cascade, making the quantum efficiency of QCLs greater than unity and leading to their high optical output power.

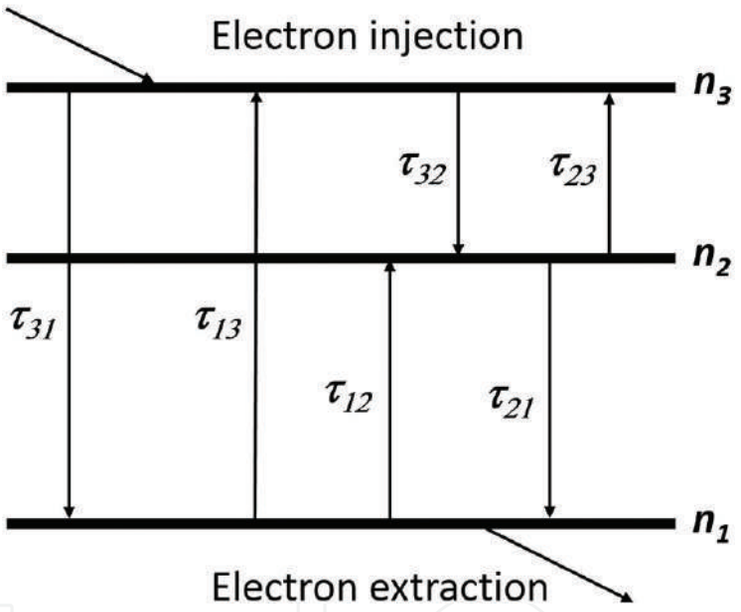

Figure 3. Three-level intersubband transition and scatterings considered in most QCLs.

QCLs are usually three-level lasers, whose level transitions are depicted in **Figure 3**. In these lasers, the wave function formation is faster than scattering between states; hence, the time-independent solutions of the Schrödinger equation can be applied, so the system can be modelled using rate equations. Each subband, i, is considered to have n_i electrons, and a scatter between the initial and the final subband, f, will have a scattering rate, W_{if}, and lifetime, τ_{if}. If no other subbands are populated, the rate equations are described as extraction and injection of electrons, respectively (depicted in **Figure 3**), whose values are both equal in steady-state conditions, where time derivatives are zero. Hence, the general rate equation for electrons in a subband i within an N level system is where $I = I_{ee} = I_{ie}$. At low temperature, absorption is near zero: hence, $\tau_{32} > \tau_{21}$, so $W_{21} > W_{32}$, and $n_3 > n_2$ leading to the existence of population inversion.

$$dn_1 / \mathrm{dt} = n_2 / \tau_{21} + n_3 / \tau_{31} - n_1 / \tau_{13} - n_1 / \tau_{12} - I_{ee} \quad (1)$$

$$dn_2 / \mathrm{dt} = n_3 / \tau_{32} + n_1 / \tau_{12} - n_2 / \tau_{21} - n_1 / \tau_{23} \quad (2)$$

$$dn_3 / \mathrm{dt} = I_{ie} + n_1 / \tau_{13} + n_2 / \tau_{23} - n_3 / \tau_{31} - n_3 / \tau_{23} \quad (3)$$

where I_{ee} and I_{ie} are the extraction and injection of electrons, respectively (depicted in **Figure 3**), whose values are both equal in steady-state conditions, where time derivatives are zero. Hence, the general rate equation for electrons in a subband i within an N level system is

$$dn_i / \mathrm{dt} = S_{f=1}^{N} n_j / \tau_{fi} - n_i S_{f=1}^{N} \tau_{if}^{-1} + \mathrm{I}(d_{i0} - d_{iN}) \quad (4)$$

where $I = I_{ee} = I_{ie}$. At low temperature, absorption is near zero:

$$n_3 / \tau_{32} = n_2 / \tau_{21} \quad (5)$$

hence, $\tau_{32} > \tau_{21}$, so $W_{21} > W_{32}$, and $n_3 > n_2$ leading to the existence of population inversion.

The scattering rate between two subbands strongly depends upon the overlap of the wave functions and energy spacing between the subbands. In order to decrease W_{32}, the overlap of the upper and lower laser levels is reduced. This is often achieved through designing the layer thickness such that the upper laser level is mostly localized in the left part of the well of the 3QWs active region, while the lower laser level wave function is made to mostly reside in the central and right part of the wells, leading to the so-called diagonal transition. A vertical transition is one which the upper laser level is rather localized in the central and right part of the wells, increasing the overlap and, therefore, W_{32}, reducing the population inversion but increasing the strength of the radiative transition and hence the gain. On the other hand, in order to increase W_{21}, the lower laser level and the ground level wave functions are designed to obtain a good overlap, and the energy spacing between the subbands is designed such that it is equal to the longitudinal optical (LO) phonon energy so that the resonant LO phonon-electron scattering can depopulate the lower laser level. For instance, the LO-phonon energy is around 36 meV in GaAs (which is comparable to the room temperature $k_B T$ value of around 26 meV) and around 91 meV in GaN [9].

Tunable semiconductor lasers can be produced by using multiple resonators or multisection injection devices [10–12]. In fact, tunable QCLs have been demonstrated [7] some time ago. Moreover, a QCL with a heterogeneous cascade containing two substacks previously optimized to emit at 5.2 and 8.0 μm, respectively, was presented by Gmachl et al. [13]. On the other hand, single-mode tunable QC distributed feedback lasers emitting between 4.6 and 4.7μm

wavelength have been reported [14]. These lasers were pulsed, continuously tunable single-mode emission and were achieved from 90 to 300 K with a tuning range of 65 nm and a peak output power of approximately 100 mW at room temperature—so the lasers described by Pellandini et al. [12], Gmachl et al. [13] and Köhler et al. [14] were laser sources for the mid-infrared region. In order to realize near-infrared QCLs, optical non-linearity in intersubband lasers has been used to design such lasers emitting at 4.76 μm, with third harmonic and second harmonic generation at 1.59 and 2.38 μm, respectively [15].

3. Materials used and growth methods

The first QCL in 1994 used InAlAs as the cladding layers due to its low refractive index of around 3.20. The core region, which includes active and injector regions, usually has 500 stacking layers consisting of alternative InGaAs and InAlAs layers with total thickness about 1.5–2.5 μm. The average refractive index in this region can be calculated according to the volume fraction of these two constituent materials and is often around 3.35, which is clearly higher than the cladding layers [16]. The confinement factor with typical Np of approximately 30 is usually around 0.5. To reduce the optical loss, the cladding layers are usually doped with a low concentration of 5×10^{16} cm^{-3} and the separate confinement heterostructures (SCHs) are implemented with InGaAs of high refractive index to increase the optical confinement factors. In later designs, the InAlAs cladding layers were replaced by InP because it has a lower refractive index of around 3.10 and a higher thermal conductivity for better heat treatment, which is a critical step for the device performance [16].

So far, the emission wavelength of QCLs has been extended from the near infrared (around 100 THz) to terahertz regimes. While the longest demonstrated wavelength is 1.6–1.8 THz with $GaAs/Al_{0.1}Ga_{0.9}As$ system at 80 K under continuous-wave (CW) operation [17], the shortest wavelength has been extended to 3 μm with $In_{0.53}Ga_{0.47}As/AlAs_{0.56}Sb_{0.44}$ system at 300 K under pulsed operation [18]. The highest output power of short-wavelength QCL (4.6 μm) under CW operation at room temperature has been demonstrated (100 mW and maximum temperature 105°C). All of these state-of-the-art QCLs have been grown by MBE so far, but for industry MOCVD is preferable for mass production. As a result, attempts have been made to grow QCLs by MOCVD. Until now, there are only three groups successfully reporting the growth of QCLs by MOCVD: an InP-based QCL ($\lambda \approx 8.5$ μm) operating in pulsed mode at room temperature, with low-temperature threshold current density in the region of 1500 A/cm^2 [19], an $In_{0.53}Ga_{0.47}As/In_{52}Al_{0.48}As$ QCL ($\lambda \approx 8.5$) operated in continuous-wave operation at room temperature with an output power of 5.3 mW [20], and Diehl et al. [21] managed to grow a QCL working in continuous-wave mode above 370 K, with an optical output power of 312 mW at room temperature and an emission wavelength of 5.29 mm. More effort is still required for MOCVD growers to develop more advanced techniques to compete with MBE. Having said that, room-temperature operation in InAs/AlSb QCLs has been achieved at 4.5 μm [22]; more recently, MBE-grown InAs/AlSb on n-InAs (100) substrate QCL operating at 8.9 μm has been reported, with a maximum operating temperature of 305 K [23].

QCLs provide one possible method of realizing high-efficiency light emitters in indirect band gap materials such as silicon. Electroluminescence at terahertz frequencies from Si/SiGe intrasubband transitions has been demonstrated [24], and recently silicide low-loss (down to 2 cm^{-1}) waveguides were designed [25, 26]. **Figure 4** shows a transmission electron microscopy (TEM) image from a Si/SiGe QCL.

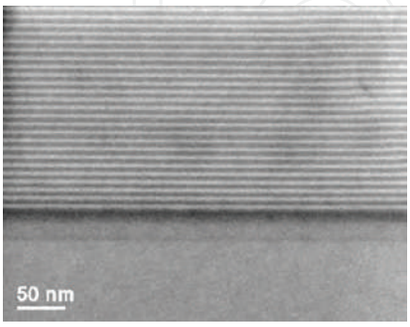

Figure 4. TEM image from a Si/SiGe quantum cascade structure, consisting of 600 periods of 6.5 nm $Si_{0.7}Ge_{0.3}$ quantum wells with 2-nm strained-Si barriers, all grown on top of a $Si_{0.8}Ge_{0.2}$ virtual substrate. The quantum cascade laser has a total thickness of 5 mm.

Although GaN-based materials have not been employed to fabricate QCLs, they are also promising materials to be used as such devices. III–V nitrides are known in their wurtzite structure to possess a large spontaneous polarization and piezoelectric constants. As a result, two-dimensional (2D) charges build up at nitride heterointerfaces where the polarization discontinuities occur, causing strong built-in electric fields [27]. Furthermore, GaN is a material with large LO-phonon energy, leading to a thermal population reduction of the lower laser state, a feature desirable for high-temperature operation of terahertz QCLs, as proposed by Diehl et al. [21]. On the other hand, ultrafast LO-phonon scattering in GAN/AlGaN QWs can be useful in order to rapidly depopulate the lower laser state [28, 29]. Lastly, the large LO-phonon energy can also increase the lifetime of the upper laser state by reducing the relaxation of electrons with higher in-plane kinetic energy via emission of a LO phonon. Using low-pressure MOCVD, GaN/AlGaN active regions for QCLs have been grown by Huang et al. [30]. GaN/AlGaN active layers are depicted in **Figure 5**.

Finally, typical phonon frequency redshift is a key indicator of good periodicity of MOVPE-grown GaN/AlGaN QCL structures, 822 cm^{-1} in the superlattice has been measured, indicating a redshift with respect to the single AlGaN layer [31].

AlN/GaN compound is another possible material to be used to fabricate quantum cascade structures. A suitable method of fabrication is hot-wall epitaxy (HWE) [32], a low-cost, convenient and scalable technique, where the epitaxial layers are grown under conditions as near as possible to thermodynamic equilibrium, allowing a minimum material loss. Inoue et al. [33] grew short-period superlattices consisting of five periods of GaN wells of 10 (or nine) molecular layers (MLs) each with 1 ML AlN barriers, which was designed to emit photons at a wavelength within the mid-infrared range (around 5 μm) [34, 35].

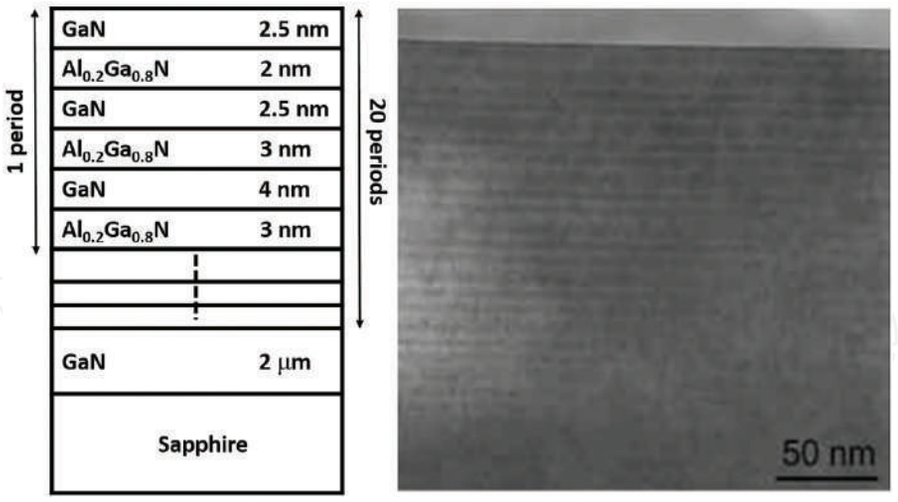

Figure 5. Schematic diagram of the AlGaN QCL active layer structure (left) and cross-sectional TEM (right) of the 20-period GaN/AlGaN MQW MQL structure.

4. Applications

We could say that QCLs, in short, are eligible to those applications where a powerful and reliable mid-infrared source is required. For instance, most chemical compounds have their fundamental modes in the mid-infrared region (3–15 μm) of the electromagnetic spectrum, thus making this range of paramount importance for gas sensing and spectroscopy applications. The so-called two 'atmospheric windows' are two windows corresponding to the ranges 3–5 and 8–12 μm, at which the atmosphere happens to show a high transparency leading to remote sensing and detection in those windows. In this section, a brief description of the current applications of QCLs is elaborated, being summarized as subsequently.

4.1. Trace-gas detection by optical methods in the mid-infrared

Most trace gases of importance, from products of fossil fuel burning to constituents of human breath, have telltale absorption features in this wavelength range, that is, their 'fingerprint' region of the spectrum, as a result of molecular rotational-vibrational transitions [16]. Narrow-linewidth, tunable semiconductor lasers in this wavelength range are used to spectrally map out and qualitatively and quantitatively detect these trace gases, by a measurement technique called tunable infrared laser diode absorption spectroscopy (TILDAS) [36]. A schematic representation of a TILDAS is shown in **Figure 6**. The advantage of TILDAS is its high sensitivity and specificity, usually combined with the advantages of the solid-state device approach.

This technique has been successfully introduced in distributed feedback quantum cascade laser (DFB-QCL) structures [37]. DFB-QCLs were first introduced in 1997 [38], providing continuously tunable single-mode laser output, and were demonstrated for the first time in

trace-gas sensing applications 1 year later [37]. DFB-QCLs operate as follows: a grating with period L is incorporated into the wavewide, lowering the threshold gain (by reducing the outcoming loss) for a different wavelength close to the Bragg wavelength:

$$\lambda = 2 \cdot n_{\text{eff}}(T) \cdot L \tag{6}$$

where n_{eff} is the effective refractive index of the waveguide mode, and is a function of temperature. As temperature increases, wavelength shifts to longer values. Changing the heat-sink temperature could control laser temperature; however, the process is slow due to the fact that it implies adiabatically temperature change of a large volume. Tuning rates increase with heat-sink temperature current from 0.3 to 0.4 nm K^{-1}, for a laser emitting at approximately 5.2 μm, and from 0.4 to 0.65 nm K^{-1}, for a laser whose emitting wavelength is around 8 μm [16].

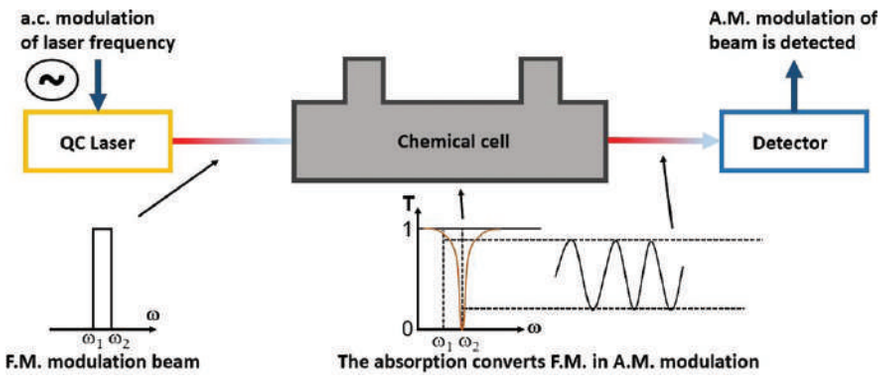

Figure 6. Depiction of a tunable infrared laser diode absorption spectroscopy (TILDAS).

4.2. Absorption measurements

In direct absorption measurements, the change in intensity of a beam is recorded as the latter crosses a sampling cell where the chemical to be detected is contained, making this measurement technique quite simple. In a version of this technique, the light interacts with the substance through the evanescent field of a waveguide or an optical fibre.

Namjou et al. [37] used the first DFB-QCL for gas detection purposes. The laser was operated at room-temperature conditions in order to measure mid-infrared (1 around 7.8 μm) absorption spectra of gases N_2O and CH_4, diluted in N_2 and prepared in a 10-cm long single pass gas cell, using a wavelength-modulation technique. The noise equivalent sensitivity limit of the measurement was 50 ppm. Sharpe et al. [39] used a DFB-QCL emitting at 5.2 and 8.5 μm to carry out direct absorption measurements of NO and NH_3, respectively. Williams et al. [40] measured the intrinsic linewidth of several DFB-QCLs emitting at around 8 μm, by observing fluctuation of the collected optical intensity when the laser beam was passing through a sample cell containing N_2O, with a well-known absorption features as the laser was being tuned to the side of one such absorption line. Finally, Kosterev et al. [41] developed a variable-duty cycle

and quasi-CW frequency-scanning technique for DFB-QCLs, which relieves many of the thermally induced effects of pulsed operation. Combining this laser with a 100-m multipass gas cell and zero-air background subtraction, a detection sensitivity close to 1 ppb concentration levels was achieved; these authors also demonstrated, by using QC-DFB lasers, high-sensitivity detection of simple molecules when a spectral resolution of approximately 300 MHz is sufficient [42].

4.3. Cavity ring-down spectroscopy

Cavity ring-down spectroscopy (CRDS) is used to measure the concentration of some light-absorbing substance, typically a gas. A short pulse of laser light is injected into the cavity, bouncing back and forth between the mirrors facing each other that make up the cavity. Typically 0.1% of the laser light comes out of the cavity and can be measured whenever the light hits one of the mirrors. Hence, as some light is lost on each reflection, the amount of light hitting the mirror decreases each time, leaking a percentage through. An absorbent medium is placed in the cavity, making light undergo fewer detections before it is extinguished. In short, CRDS measures the time it takes for the light to drop for a certain percentage of its original amount, and this ring-down time can be converted to a concentration, having two main advantages: fluctuations in the laser do not affect the measurement (the ring-down time does not depend upon the brightness of the laser), and due to its long pathlength, it is very sensitive, since the light reflects many times between the mirrors.

Paldus et al. [43] reported the use of a 126 mW CW operated DFB-QCL emitting at around 8.5 μm for CRDS of ammonia diluted in nitrogen. A sensitivity of 3.4×10^{-9} cm^{-1} Hz-1/2 was achieved for ammonia in nitrogen at standard temperature and pressure, which corresponds to a detection limit of 0.25 ppbv.

4.4. Photoacoustic spectroscopy

The photoacoustic effect was discovered in 1880 by Alexander Graham Bell, who showed that thin discs emit sound when exposed to a beam of sunlight that was quickly interrupted with a rotating slotted disc. The absorbed energy from the light was transformed into kinetic energy in the sample and so a local heating and a pressure wave of sound arose. Later, Bell demonstrated the fact that materials exposed to different regions of the solar spectrum, that is, infrared and ultraviolet, can produce sounds too. Hence, by measuring the sound at different wavelengths, a photoacoustic spectrum from a sample can be recorded, so that it can be used to identify the absorbing components of the sample. This technique can be used to study solids, liquids and gases.

One of the uses of photoacoustic spectroscopy is the study of gas concentrations at the parts per billion or even parts per trillion levels. Although most photoacoustic detectors do not differ much from the original Bell's set-up, some enhancements have been incorporated in order to increase the sensitivity, such as enclosing the gaseous sample in a cylindrical chamber, and amplifying the sound signal by tuning the modulation frequency to an acoustic resonance of

the sample cell, by using high-sensitive microphones together with lock-in techniques and utilizing intense lasers instead of sunlight to illuminate the sample.

Paldus et al. [44] reported photoacoustic spectroscopy on NH_3 and H_2O diluted in N_2 using a CW DFB-QCL emitting at a wavelength of 8.5 μm. The noise-limited minimum detectable concentration of NH_3 was 100 ppbv for an integration time of 1 s. Lastly, Nägele et al. [45] built a multicomponent (ethane, methanol and ethanol) trace-gas monitoring system using QCLs as pump sources and a multipass photoacoustic cell.

4.5. Other spectroscopies

Other types of spectroscopies have also been used in the context of QCLs detection.

First, lamb-dip spectroscopy is a useful technique to study the spectra from polyatomic molecules. When a monochromatic light with a given wavelength passes through a chemical cell in a set-up similar to that depicted in **Figure 6**, a Gaussian absorption spectrum centred in the wavelength comes up. If we measure the absorption of a light beam (probe beam) by passing through two beams (pump and probe beams) of the same wavelength from opposite directions, by using a beam splitter, a less intense absorption is observed at that wavelength. This reduction in intensity appears as a dip, the so-called lamb-dip, and its position gives the location of the transition wavelength having no Doppler shift (Doppler-free in the absorption curve). Samman et al. [46] used a CW-operated DFB-QCL emitting at around 5.2 mm to obtain sub-Doppler resolution-limited saturation features in a lamb-dip experiment on NO. These lamb dips appeared as transition spikes with full-width at half maximum (FWHM) values around 4.3 MHz.

Gittins et al. [47] used a multimode Fabry-Perot-type QCL emitting at around 8.0 μm wavelength for quantitative backscatter absorption measurements on isopropanol vapour. They developed and employed a pseudorandom code modulation of the laser, and explored its use for different absorption LIDAR (laser infrared detection and ranging).

Finally, Sonnenfroh et al. [48] used DFB-QCLs (1 around 5.4 μm) in quasi-CW mode close to room temperature in conjunction with a balanced radiometric detection technique to achieve high sensitivity, whereas Hvozdara et al. [49] demonstrated the first use of a GaAs-based QCL for gas-sensing applications.

4.6. Direct detection applications: drug, explosive, plasma species and aerospace and military

Drug detection is another important application field of QCL-based detection systems [50]. Lu et al. [51] demonstrated, by integrating an optoelectronic terahertz microsource into a glass-substrated microchip within the near-field distance, a compact, label-free and non-invasive microbiosensing terahertz device that allowed detection of illicit drug powders with weight in the order of the nanogram.

The detection of explosive fingerprints is of great importance for security reasons. The detection of such substances has a number of drawbacks as explosive molecules are heavy,

complex and have thousands of rotational and vibrational transitions. Furthermore, broadband features with no separation observed at low pressures happen in measured transmission spectra. Different explosives have, therefore, unique terahertz spectral fingerprints. Williams et al. [52] developed a high-power QCL emitting at around 4.4 THz. These lasers are based on a resonant-phonon depopulation scheme, and use a semi-insulating surface-plasmon waveguide. They managed a maximum power of ~248 and 138 mW pulsed and CW, respectively. van Neste et al. [53] have used two QCLs operating simultaneously with tunable wavelength windows matching the absorption peaks of analytes in order to improve sensitivities of standoff spectroscopy techniques, leading to a sensitivity of 100 ng/cm^2 and a standoff detection distance of 20 m for surface-adsorbed analytes such as explosives and tributyl phosphate.

Molecular plasmas are tools in plasma-enhanced chemical vapour deposition and in etching systems to deposit or remove thin films. The analysis of the precursor gas fragmentation and the monitoring of plasma reaction products is the key to an improved understanding and control of these chemical-active discharges. This observation can be done by using absorption spectroscopy methods in the mid-infrared spectral region. Recently, a QCL-based absorption spectroscopic system, the quantum cascade laser measurement and control system (Q-MACS), was developed and used to study industrial process plasmas and for environmental studies, and its applicability for monitoring online processes has been proven [54].

Finally, QCLs are also applied to aerospace and military uses. For instance, the first of a new generation of miniature tunable laser mid-IR spectrometers operating at room temperature for in situ measurement of atmospheric and evolved planetary gases started to develop not too long ago. These devices are based on newly available room-temperature QCL sources in the 3–12μm wavelength region and have immediate applications to Mars, Titan, Venus and Europa missions, being operated on a descending or penetrating probe, lander, rover or aerobot, and would consume only a few watts of power, with a weight less than 1 kg [55]. Furthermore, features of QCL make them good laser sources to carry out non-destructive-imaging engine combustors, where failure mechanisms, engine performance in aircraft and moisture content in jet fuel are examined. A low thermal noise background is required for such purpose, and ceramic ports exist already on such platforms transparent to terahertz radiation. Scale model radar cross-section experiments have also been carried out in the aerospace industry, to replace the bulky and extremely inefficient molecular lasers with QCLs, at the University of Massachusetts Lowell Sub-Millimetre Wave Laboratory [56], to perform scale model radar cross-section measurements for phenomenology and target-recognition database formation.

The infrared spectrum is also used in the aerospace industry for detection purposes, for instance, in the infrared scene generation, which is presently a critical technology for testing of infrared-imaging systems, for example, in infrared-guided missile systems, and QCLs could have an application in this technology to replace large- and slow-response 'resistor banks' with tailored design QCLs, to mimic the thermal background of a given scene [57]. Moreover, coherent transceiver using a terahertz quantum cascade laser (TQCL) as the transmitter and an optically pumped molecular laser as the local oscillator has been used for imaging purposes along with inverse synthetic aperture radar (ISAR), in which the range of the target was limited

by the TQCL power (around 10–4 W) and indoor atmospheric attenuation at 2.408 THz, leading to a coherence length of the transmitter of up to several hundred metres [58].

5. State of the art and outlook

QCLs are also currently facing a number of challenges, which will be summarized below.

First, the extensions of the wavelength range into the far-infrared. Rochat et al. [59] grew far-infrared QC structures based on a vertical transition active region emitting at l around 76 μm. This is a challenging issue, so long as population inversion is difficult to attain for such long wavelengths. Energy levels are generally so close that selective injection into a single level is difficult. Furthermore, LO-phonon scattering is replaced by electron-electron scattering as the dominant electron relaxation mechanism, which is more difficult to model accurately. Moreover, wavewide losses are expected to be high, although even very low-temperature QCL operation would be a great accomplishment due to the lack of narrow band and high-power compact sources in the far-infrared wavelength range. In fact, temperature is a key player when it is required to achieve a certain emission wavelength as **Figure 7** shows.

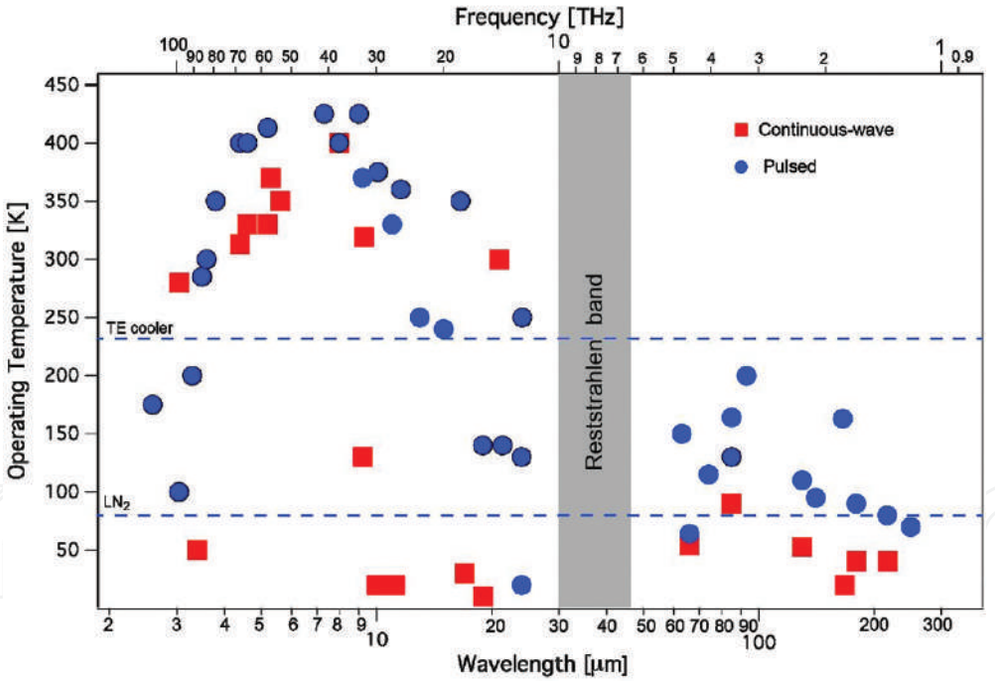

Figure 7. Operating temperature plot as a function of the emission wavelength/frequency for QCLs [60].

Another challenge would also be to fibre-optic wavelengths. In fact, the fabrication of large optical waveguides, powers of 14 and 5 W at respective temperatures of 15 and 280 K, is demonstrated at a wavelength of approximately 5.2 μm [61].

On the other side of the IR spectrum, reaching shorter wavelengths is another motivation for a more selection of materials. Work on this respect has also be done on GaN-based devices [61],

with Gmachl et al. [62] having measured intersubband optical absorption in narrow (15–30 Å wide), GaN/AlGaN quantum wells grown by MBE on sapphire substrate. Peak absorption wavelengths ranged from 4.2 μm for 30Å wide wells to 1.77 μm for a 15Å wide well. On the other hand, Iizuka et al. [63] reported ultrafast intersubband relaxation (less than 150 fs) at a wavelength of 4.5 μm in $Al_{0.65}Ga_{0.35}N$/GaN MQWs, with as many as 200 QWs, making this result promising for fabrication ultrafast optical switches.

Doping level of the active region is a key optimization parameter that determines maximum drive current, optical losses and threshold current. Faist et al. [61] presented a systematic change of the active region doping in an InAlAs-InGaAs/InP lasers emitting at 9 μm. On the other hand, the wavelength tunability of each QC-DFB laser is especially limited to cover the entire molecular absorption spectrum of volatile organic compounds and hydrocarbons, which could be addressed by separating the gain medium from the wavelength-selective element [61].

Other challenges involve the low conversion efficiencies (<1%) between electrical and optical power, also known as wall plug efficiency (WPE) [64], and also the unavoidable fact that far-infrared (terahertz) QCLs lack proper performance at room-temperature operation. Belkin et al. [65] have recently reviewed recent research that has led to a new class of QCL light sources that has overcome these limitations leading to room-temperature operation in the terahertz spectral range, with nearly 2 mW of optical power and significant tunability by using intra-cavity THz difference-frequency generation (DFG) in dual-wavelength mid-IR QCLs. However, Lu et al. [66] recently presented a strong-coupled strain-balanced quantum cascade laser design for efficient THz generation based on intra-cavity difference-frequency generation, demonstrating continuous-wave, single-mode THz emissions with a wide-frequency tuning range of 2.06–4.35 THz and an output power up to 4.2 μW at room temperature from two monolithic three-section sampled grating distributed feedback-distributed Bragg reflector lasers.

Furthermore, Burghoff et al. [67] demonstrated frequency combs based on terahertz QCLs, combining high power of lasers with the broadband capabilities of pulsed sources. By fully exploiting the quantum-mechanically broadened gain spectrum available to these lasers, 5 mW of terahertz power spread across 70 laser lines can be generated. Therefore, the radiation is sufficiently powerful to be detected by Schottky-diode mixers, and will lead to compact terahertz spectrometers.

About gas detection, Harrer et al. [68] combined the operation mode and low-divergence emission from QCLs with two-dimensional array integration with multiple emission and detection frequencies leading to detecting propane concentrations of 0–70 and 0–90% for isobutane at a laser operation wavelength of 6.5 μm using a 10 cm gas cell in double-pass configuration.

Finally, possibly the best way to assess the current state of the art for volume production of QCLs is to start from the market requirement from the end-user point of view. An example is the continuous emission monitoring (CEM) market, which includes engine emission and power-plant stack monitoring, is fiercely competitive, with a range of different gas-sensing technologies, such as Fourier transform spectrometry, chemiluminescence, non-dispersive

infrared, and so on, each trying to increase its market share. Among these technologies, QCL-based gas sensor technology is still in its infancy, since although predictions indicate a great improvement in performance, much demonstration and convincing is still required in this conservative market. Moreover, it is difficult to justify a system whose price is above the market, despite better performance, due to the risk of an unproven and new technology. Hence, a QCL device might be priced below the market, which can have negative consequences that can reach the component supplier. Customers are usually reluctant to acquire a new sensor having other well-proven systems already in the market. Therefore, demonstration of the unique advantages of the QCL-based devices is often necessary, including specifications, performance, mean time to failure (MTTF) parameters, traceability and warranty period with a significant impact [69]. Implementation of high-volume production and proper validation processes on QCLs are producing positive outcomes. Along with a noticeable improvement in gas-sensing performance parameters, volume-cost reduction is allowing QCL systems price decrease to meet market demands. By consistently tackling the challenges of the QCL volume manufacturing, carrying out severe testing procedures, implementing quality-control systems and reaching adequate device costing, QCL developers and manufacturers can complete and come into the marketplace.

Finally, continuing to build consumer confidence in QCL commercial products, it should be easier for customers to digest the unavoidable contract 'warranty' and 'product liability' clauses found in supply contracts [69].

6. Summary

In this chapter, an overview of quantum cascade lasers (QCLs) is presented. A historical introduction is first introduced. The basic features of QCLs are outlined, as well as a brief description of the issues that this work deals with. The operation and fundamentals of QCLs are also described. An analysis of the operation of these structures is included. Basically, the use of superlattices and tunability due to the layer thickness are the key features, in conjunction with the intersubband tunnelling transition – cascade. The QCLs are usually three-level lasers. Rate equations are also included. Furthermore, introducing a graphical brief timeline (**Figure 8**), including some of the most important milestones achieved in the world of QCL, would be helpful in this section.

An overview over the materials used for these devices is also included, that is, InGaAs and InAlAs layers, InAs/AlSb, Si/SiGe and GaN-based.

QCLs have a wide range of applications: first, trace-gas detection by optical methods in the mid-infrared, the great suitability of the TILDAS techniques and DFB-QCLs in trace-gas-sensing applications.

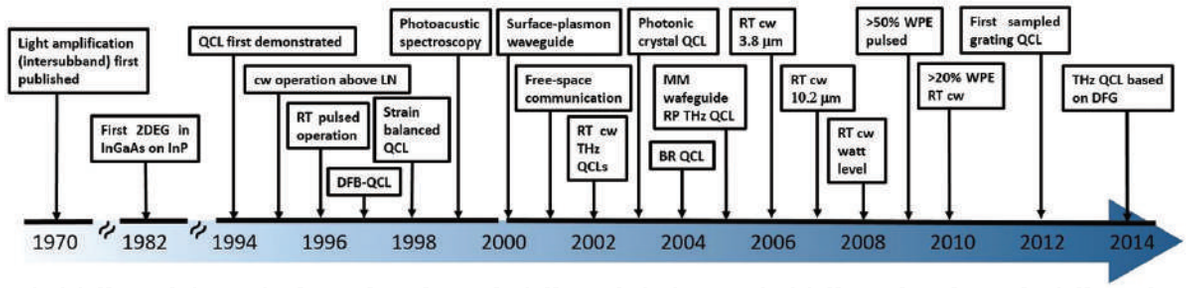

Figure 8. Achievements of QCLs over time.

Cavity ring-down spectroscopy is another technique used for gas detection and briefly described above. QCLs are also applied in photoacoustic spectroscopy, to study gas concentrations at the parts per billion or even parts per trillion levels. Applications in gas detection using QCLs with other types of spectroscopy and variations, such as lamb-dip spectroscopy, radiometric detection techniques, and so on, are mentioned.

The latest advances in QCL applications are also described. The extension of the wavelength range into the far-infrared but also shorter wavelengths, fibre-optic wavelengths and fabrication of large optical waveguides, doping issues, room-temperature operation problems, frequency combs based on terahertz devices, new insights on gas detection and finally current state of the art for volume production of QCLs are mentioned.

Author details

Raúl Pecharromán-Gallego*

Address all correspondence to: anubis_rpg@hotmail.com

The Last Push Consulting, Heverlee, Leuven, Belgium

References

[1] Esaki L, Tsu R. Superlattice and negative differential conductivity in semiconductors. IBM Journal of Research and Development. 1970;14(1):61–65. DOI: 10.1147/rd.141.0061.

[2] Kazarinov R, Suris R. Possibility of the amplification of electromagnetic waves in a semiconductor with a superlattice. Soviet Physics—Semiconductors. 1971;5(4):707–709.

[3] Faist J, Capasso F, Sivco D L, Sirtori C, Hutchinson A L, Cho A Y. Quantum cascade laser. Science. 1994;264:553–556. DOI: 10.1126/science.264.5158.553.

[4] Markus-Christian Amann. Semiconductor Technology (E26) [Internet]. [Updated: 2016]. Available from: https://www.wsi.tum.de/Research/AmanngroupE26/AreasofResearch/tabid/115/Default.aspx [Accessed: 12-05-2016].

[5] Capasso F, Gmachl C, Sivco D L, Cho Q Y. Quantum cascade lasers. Physics World. 1999;12(6):27–33. DOI: http://dx.doi.org/10.1088/2058-7058/12/6/26.

[6] Alpes Lasers SA. Alpes Lasers—Quantum Cascade Lasers [Internet]. [Updated: 2016]. Available from: http://www.alpeslasers.ch/ [Accessed: 12-05-2016].

[7] Tredicucci A, Gmachl C, Capasso F, Sivco D L, Hutchinson A L, Cho A Y. A multiwavelength semiconductor laser. Nature. 1998;396:350–353. DOI: 10.1038/24585.

[8] Kosterev A A, Tittel F K, Köhler R, Gmachl C, Capasso F, Sivco D L, Cho A Y, Wehe S, Allen M G. Thermoelectrically cooled quantum-cascade-laser-based sensor for the continuous monitoring of ambient atmospheric carbon monoxide. Applied Optics. 2002;41(6):1169–1173. DOI: 10.1364/AO.41.001169.

[9] Edgar J H, Strite S, Akasaki I, Amano H, Wetzel C, editors. Properties processing and applications of gallium nitride and related semiconductors. 1st ed. UK: EMIS datareviews series no 23. INSPEC; 1999. 830 p. DOI: ISBN-10: 0852969538. ISBN-13: 978-0852969533.

[10] Beernik K J, Thornton R L, Chung H F. Low threshold current dual wavelength planar buried heterostructure lasers with close spatial and large spectral separation. Applied Physics Letters. 1994;64(9):1082–1084. DOI: 10.1063/1.110939.

[11] Dutta N K, Cella T, Zilko J L, Ackerman D A, Piccirilli A B, Greene L I. InGaAsP closely spaced dual wavelength laser. Applied Physics Letters. 1986;48(25):1725–1726. DOI: 10.1063/1.96815.

[12] Pellandini P, Stanley R P, Houdre R, Oesterle U, Ilegems M, Weisbuch C. Dual-wavelength laser emission from a coupled semiconductor microcavity. Applied Physics Letters. 1997;71(7):864–866. DOI: 10.1063/1.119671.

[13] Gmachl C, Sivco D L, Baillargeon J N, Hutchinson A L, Capasso F, Cho A Y. Quantum cascade lasers with a heterogeneous cascade: two-wavelength operation. Applied Physics Letters. 2001;79(5):572–574. DOI: 10.1063/1.1383806.

[14] #Köhler R, Gmachl C, Tredicucci A, Capasso F, Sivco D L, Chu S N G, Cho A Y. Single-mode tunable, pulsed, and continuous wave quantum-cascade distributed feedback lasers at $\lambda \cong 4.6–4.7$ μm. Applied Physics Letters. 2000;79(9):1092–1094. DOI: 10.1063/1.125987.

[15] Banerjee S, Spencer P S, Shore K A. Design of a tunable quantum cascade laser with enhanced optical non-linearities. IEE Proceedings Optoelectronics. 2006;153(1):40–42. DOI: 10.1049/ip-opt:20050061.

[16] Gmachl C, Capasso F, Sivco D L, Cho A Y. Recent progress in quantum cascade lasers and applications. Report on Progress in Physics. 2001;64(11):1533–1601. DOI: 10.1088/0034-4885/64/11/204.

[17] Walther C, Scalari G, Faist J, Beere H, Ritchie D. Low frequency terahertz quantum cascade laser operating from 1.6 to 1.8THz. Applied Physics Letters. 2006;89(23): 231121–3. DOI: 10.1063/1.2404598.

[18] Revin D G, Cockburn J W, Steer M J, Airey R J, Hopkinson M, Krysa A B, Wilson R, Menzel S. InGaAs/AlAsSb/InP quantum cascade lasers operating at wavelengths close to 3 μm. Applied Physics Letters. 2007;90(2):021108–3. DOI: 10.1063/1.2431035.

[19] Green R, Roberts J, Krysa A, Wilson L, Cockburn J, Revin D, Zibik E, Carder D, Airey P. MOVPE grown quantum cascade lasers. Physica E: Low-dimensional Systems and Nanostructures. 2004;21(2-4):863–866. DOI: 10.1016/j.physe.2003.11.133.

[20] Liu Z., Wasserman D, Howard S S, Hoffman A J, Gmachl C F, Wang X, Tanbun-Ek T, Cheng L, Choa F-S. Room-temperature continuous-wave quantum cascade lasers grown by MOCVD without lateral regrowth. IEEE Photonics Technology Letters. 2006;18(12):1347–1349. DOI: 10.1109/LPT.2006.877006.

[21] Diehl L, Bour D, Corzine S, Zhu J, Höfler G, Lončar M, Troccoli M, Capasso F. High-temperature continuous wave operation of strain-balanced quantum cascade lasers grown by metal organic vapor-phase epitaxy. Applied Physics Letters. 2006;89(8): 081101–3. DOI: 10.1063/1.2337284.

[22] Teissier R, Barate D, Vicet A, Alibert C, Baranov B A, Marcadet X, Renard X, Garcia M, Sirtori C, Revin D, Cockburn J. Room temperature operation of InAs/AlSb. Applied Physics Letter. 2004;85(2):167–169. DOI: 10.1063/1.1768306.

[23] Ohtani K, Fujita K, Ohno H. Room-temperature InAs/AlSb quantum-cascade laser operating at 8.9 μm. Electronics Letters. 2007;43(9):520–522. DOI: 10.1049/el:20070251.

[24] Lynch S A, Bates R, Paul D J, Norris D J, Cullis A G, Ikonic Z, Kelsall R W, Harrison P, Arnone D D, Pidgeon C R. Intersubband electroluminescence from Si/SiGe cascade emitters at terahertz frequencies. Applied Physics Letters. 2002;81(9):1543–1545. DOI: 10.1063/1.1501759.

[25] De Rossi A, Carras M, Paul D J. Low-loss surface-mode waveguides for terahertz Si–SiGe quantum cascade lasers. IEEE Journal of Quantum Electronics. 2006;42(2):1233–1238. DOI: 10.1109/JQE.2006.883496.

[26] Paul D J. Si/SiGe heterostructures: from material and physics to devices and circuits. Semiconductor Science and Technology. 2004;19(10):75–108. DOI: 10.1088/0268-1242/19/10/R02.

[27] Pecharromán-Gallego R. Investigations of the luminescence of GaN and InGaN/GaN quantum wells [thesis]. UK: University of Strathclyde; 2004. 216 p. Available from: http://suprimo.lib.strath.ac.uk/primo_library/libweb/action/display.do?tabs=detailsTab&ct=display&fn=search&doc=SUVOY682303&indx=1&recIds=SUVOY682303&recIdxs=0&elementId=0&renderMode=poppedOut&displayMode=full&frbrVersion=&dscnt=1&scp.scps=scope%3A%28SU%29%2Cscope%3A%28cla%29&frbg=&tab=local&dstmp=1463141375653&srt=rank&mode=Ba-

sic&dum=true&tb=t&vl(freeText0)=Pecharroman&vid=SUVU01 DOI: Thesis no : T10902.

[28] Sun G, Soref R A, Khurgin J B. Active region design of a terahertz GaN/Al0.15Ga0.85N quantum cascade laser. Superlattices and Microstructures. 2005;37(2):107–113. DOI: 10.1016/j.spmi.2004.09.046.

[29] Heber J D, Gmachl C, Ng H M, Cho A Y. Comparative study of ultrafast intersubband electron scattering times at ~1.55 μm. Applied Physics Letters. 2002;81(7):1237–1239. DOI: 10.1063/1.1500412.

[30] Huang G S, Lu T C, Yao H H, Kuo H C, Wang S C, Sun G, Lin C-W, Chang L, Soref R A. GaN/AlGaN active regions for terahertz quantum cascade lasers grown by low-pressure metal organic vapor deposition. Journal of Crystal Growth. 2007;298(1):687–390. DOI: 10.1016/j.jcrysgro.2006.10.106.

[31] Wang S C, Soref R, Sun G. Fabrication and characteristics of GaN/AlGaN multilayer structure for terahertz quantum-cascade laser. SPIE Proceedings. Terahertz Physics, Devices, and Systems. 2006;6373:637309. DOI: 10.1117/12.685678.

[32] Lopez-Otero A. Hot wall epitaxy. Thin Solid Films. 1978;49(1):3–57. DOI: 10.1016/0040-6090(78)90309-7.

[33] Inoue Y, Nagasawa H, Sone N, Ishino K, Ishida A, Fujiyasu H, Kim J J, Makino H, Yao T, Sakakibara S, Kuwabara M. Fabrication and characterization of short period AlN/GaN quantum cascade laser structures. Journal of Crystal Growth. 2004;265(1-2): 65–70. DOI: 10.1016/j.jcrysgro.2004.01.044.

[34] Ishida A, Ose T, Nagasawa H, Ishino K, Inoue Y, Fujiyasu H. Quantum-cascade structure in AlN/GaN system assisted by piezo-electric effect. Japanese Journal of Applied Physics. 2002;41(2, 3A):236–238. DOI: 10.1143/JJAP.41.L236.

[35] Ishida A, Ose T, Nagasawa H, Inoue Y, Tatsuoka H, Fujiyasu H, Ko H-J, Makino H, Yao T, Kan H. Characterization of AlN/GaN quantum-cascade structures prepared by hot-wall epitaxy. Physica Status Solidi C: Current Topics in Solid State Physics. 2002;0(1): 520–523. DOI: 10.1002/pssc.200390103.

[36] Sigrist M W, editor. Air monitoring by spectroscopic techniques. United States: New York, NY: Wiley-Interscience; 1994. 531 p. DOI: ISBN 0471558753, 9780471558750.

[37] Namjou K, Cai S, Whittaker E A, Faist J, Gmachl C, Capasso F, Sivco D L, Cho A Y. Sensitive absorption spectroscopy with a room-temperature distributed-feedback quantum-cascade laser. Optics Letters. 1998;23(3):219–221. DOI: 10.1364/OL.23.000219.

[38] Faist J, Gmachl C, Capasso F, Sirtori C, Sivco D L, Billargeon J N, Cho A Y. Distributed feedback quantum cascade lasers. Applied Physics Letters. 1997;70(20):2670–2673. DOI: 10.1063/1.119208.

[39] Sharpe S W, Kelly J F, Hartman J S, Gmachl C, Capasso F, Sivco D L, Baillargeon J N, Cho A Y. High-resolution (Doppler-limited) spectroscopy using quantum-cascade

distributed-feedback lasers. Optics Letters. 1998;23(17):1396–1398. DOI: 10.1364/OL.23.001396.

[40] Williams R M, Kelly J F, Hartman J S, Sharpe S W, Taubman M S, Hall J L, Capasso F, Gmachl C, Sivco D L, Baillargeon J N, Cho A Y. Kilohertz linewidth from frequency-stabilized mid-infrared quantum cascade lasers. Optics Letters. 1999;24(24):1844–1866. DOI: 10.1364/OL.24.001844.

[41] Kosterev A A, Curl R F, Tittel F K, Gmachl C, Capasso F, Sivco D, Baillargeon J N, Hutchinson A L, Cho A Y. Effective utilization of quantum-cascade distributed-feedback lasers in absorption spectroscopy. Applied Optics. 2000;39(24):4425–4430. DOI: 10.1364/AO.39.004425.

[42] Kosterev A A, Curl R F, Tittel F K, Gmachl C, Capasso F, Sivco D L, Baillargeon J N, Hutchinson A L, Cho A Y. Absorption spectroscopy with quantum cascade lasers. Laser Physics. 2001;11(1):39–49. DOI: PMID 12143896.

[43] Paldus B A, Harb C C, Spence T G, Zare R N, Gmachl C, Capasso F, Sivco D L, BaillargeonJ N, Hutchinson A L, Cho A Y. Cavity ringdown spectroscopy using mid-infrared quantum-cascade lasers. Optics Letters. 2000;25(9):666–668. DOI: 10.1364/OL.25.000666.

[44] Paldus B A, Spence T G, Zare R N, Oomens J, Harren F J M, Parker D H, Gmachl C, Cappasso F, Sivco D L, Baillargeon J N, Hutchinson A L, Cho A Y. Photoacoustic spectroscopy using quantum-cascade lasers. Optics Letters. 1999;24(3):178–180. DOI: 10.1364/OL.24.000178.

[45] Nägele M, Hofstetter D, Faist J, Sigrist M W. Mobile laser photoacoustic spectrometer for multicomponent trace-gas monitoring based on CO_2- and quantum-cascade lasers as pump sources. In: Conference on Lasers and Electro-Optics Europe; 10–15 September, 2000; Nice, France. IEEE; 2000. p. 12–22. DOI: 10.1109/CLEOE.2000.909779.

[46] Samman A, Rimai L, McBride J R, Carter R O, Weber W H, Gmachl C, Capasso F, Hutchinson A L, Sivco D L, Cho A Y. Potential use of near, mid and far infrared laser diodes in automotive LIDAR applications. In: 52nd Vehicular Technology Conference; 24–28 September, 2000; Boston. USA. IEEE; 2000. p. 2084–2089, vol. 5. DOI: 10.1109/VETECF.2000.883239.

[47] Gittins C M, Wetjen E T, Gmachl C, Capasso F, Hutchinson A L, Sivco D L, Baillargeon J N, Cho A Y. Quantitative gas sensing by backscatter-absorption measurements of a pseudorandom code modulated $\lambda \sim 8$-μm quantum cascade laser. Optics Letters. 2000;25(16):1162–1164. DOI: 10.1364/OL.25.001162.

[48] Sonnenfroh D M, Rawlins W T, Allen M G, Gmachl C, Capasso F, Hutchinson A L, Sivco D L, Baillargeon J N, Cho A Y. Application of balanced detection to absorption measurements of trace gases with room-temperature, quasi-CW quantum-cascade lasers. Applied Optics. 2001;40(6):812–820. DOI: 10.1364/AO.40.000812.

[49] Hvozdara L, Gianordoli S, Strasser G, Schrenk W, Unterrainer K, Gornik E, Murthy C S S S, Kraft M, Pustogow V, Mizaikoff B, Inberg A, Croitoru N. Spectroscopy in the gas phase with GaAs/AlGaAs quantum-cascade lasers. Applied Optics. 2000;39(36):6926–6930. DOI: 10.1364/AO.39.006926.

[50] Kawase K. Terahertz imaging for drug detection and large-scale integrated circuit inspection. Optics and Photonics News. 2004;15(10):34–39. DOI: 10.1364/OPN.15.10.000034.

[51] Lu J Y, Chen L J, Kao T F, Chang H H, Chen H W, Liu A S, Chen Y C, Wu R B, Liu W S, Chyi J I, Sun C K. Terahertz microchip for illicit drug detection. IEEE Photonics Technology Letters. 2006;18(21):2254–2256. DOI: 10.1109/LPT.2006.883285.

[52] Williams B S, Kumar S, Hu Q, Reno J L. High-power terahertz quantum-cascade lasers. Electronics Letters. 2006;42(2):89–91. DOI: 10.1049/el:20063921.

[53] van Neste C W, Senesac L R, Thundat T. Standoff spectroscopy of surface adsorbed chemicals. Analytical Chemistry. 2009;81(5):1952–1956. DOI: 10.1021/ac802364e.

[54] Röpcke J, Davies P B, Glitsch S, Hempel F, Macherius U, Lang N, Rousseau A, Stancu G D, Weltmann K-D, Welzel S, Zimmermann H. Q-MACS, A compact quantum cascade laser absorption spectroscopy system for plasma diagnostics. In: The 2nd International Workshop on Quantum Cascade Lasers; 6–9 September 2006; Brindisi, Italy. Massachusetts Institute of Technology; 2006. p. 388–395.

[55] Jet Propulsion Laboratory. Mars Science Laboratory [Internet]. Available from: http://mars.jpl.nasa.gov/msl/ [Accessed: 19-05-2016].

[56] University of Massachusetts Lowell Sub-Millimetre Wave Laboratory. Sub-Millimetre Wave Laboratory | UMass Lowell [Internet]. Available from: https://www.uml.edu/Research/STL/ [Accessed: 19-05-2016].

[57] Nelson T R. USAF applications for quantum cascade lasers. In: The 2nd International Workshop on Quantum Cascade Lasers; 6–9 September 2006; Brindisi, Italy. Massachusetts Institute of Technology; 2006. p. 455–465.

[58] Danylov A A, Goyette T M, Waldman J, Coulombe M J, Gatesman A J, Giles R H, Qian X, Chandrayan N, Vangala S, Termkoa K, Goodhue W D, Nixon W E. Terahertz inverse synthetic aperture radar (ISAR) imaging with a quantum cascade laser transmitter. Optics Express. 2010;18(15):16264–16272. DOI: 10.1364/OE.18.016264.

[59] Rochat M, Beck M, Faist J, Oesterle U. Measurement of far-infrared waveguide loss using a multisection single-pass technique. Applied Physics Letters. 2001;78(14):1967–1969. DOI: 10.1063/1.1357444.

[60] Vitiello M S, Scalari G, Williams B, Paolo D-N. Quantum cascade lasers: 20 years of challenges. Optics Express. 2015;23(4):5167–5182. DOI: 10.1364/OE.23.005167.

[61] Faist J, Aellen T, Gresch T, Beck M, Giovannini M. Mid-infrared coherent sources and applications. NATO Science for Peace and Security Series ed. The Netherlands: Springer; 2008. 630 p. DOI: ISBN: 978-1-4020-6463-0.

[62] Gmachl C, Ng H M, Cho A Y. Intersubband absorption in GaN/AlGaN multiple quantum wells in the wavelength range of $\lambda \sim 1.75–4.2$ μm. Applied Physics Letters. 2000;77(3):334–336. DOI: 10.1063/1.126968.

[63] Iizuka N, Kaneko K, Suzuki N, Asano T, Noda S, Wada O. Ultrafast intersubband relaxation (≤150 fs) in AlGaN/GaN multiple quantum wells. Applied Physics Letters. 2000;77(5):648–650. DOI: 10.1063/1.127073.

[64] Yao A Y, Hoffman J, Gmachl C. Mid-infrared quantum cascade lasers. Nature Photonics. 2012;6(7):432–439. DOI: 10.1038/nphoton.2012.143.

[65] Belkin M A, Capasso F. New frontiers in quantum cascade lasers: high performance room temperature terahertz sources. Physica Scripta. 2015;90(11):118002. DOI: 10.1088/0031-8949/90/11/118002.

[66] Lu Q, Wu D, Sengupta, Slivken S, Razeghi M. Room temperature continuous wave, monolithic tunable THz sources based on highly efficient mid-infrared quantum cascade lasers. Scientific Reports. 2016;6:23595. DOI: 10.1038/srep23595.

[67] Burghoff D, Kao T-Y, Han N, Chan C W I, Cai X, Yang Y, Hayton D J, Gao J-R, Reno J L, Hu Q. Terahertz laser frequency combs. Nature Photonics. 2014;8:462–467. DOI: 10.1038/nphoton.2014.85.

[68] Harrer A, Szedlak R, Schwarz B, Moser H, Zederbauer T, MacFarland D, Detz H, Andrews A M, Schrenk W, Lendl B. Mid-infrared surface transmitting and detecting quantum cascade device for gas-sensing. Scientific Reports. 2016;6:21795. DOI: 10.1038/srep21795.

[69] Normand E, Howieson I. Quantum-cascade lasers enable gas-sensing technology. Laser Focus World. 2007;43(4):90–92.

Chapter 2

Electronic Band Structure of Quantum Cascade Laser

Arpan Deyasi

Additional information is available at the end of the chapter

http://dx.doi.org/10.5772/66942

Abstract

Multiple quantum well structure is the subject of theoretical and experimental research over the last two decades due to the possibility of making novel electronic and optoelectronic devices. The phenomenon of resonant tunneling makes it a prime candidate for all tunneling-based quantum devices with one-dimensional confinement. THz laser design using multilayered low-dimensional semiconductor structure is one such example, where miniband formation and its energy difference with lowest quantum state play crucial factor in governing device performance. Quantum cascade laser (QCL) is one of such candidate, which speaks in favor of research using multiple-quantum-well (MQW) structure. In the proposed chapter, transmission coefficient of multiple quantum-well structure is numerically computed using propagation matrix technique, and its density of states is calculated in the presence and absence of electric field applied along the direction of quantum confinement. Absorption coefficient is also calculated for its possible application as optical emitter/detector. Based on the electronic and photonic properties investigated, electronic band structure of the quantum cascade laser (formed using the MQW structure) is computed. Formation of miniband is tailored with variation of external bias is shown.

Keywords: multiple quantum well, electronic band structure, quantum cascade laser, miniband, band nonparabolicity, electric field

1. Introduction

Research in the area of nanostructures, more precisely on optoelectronic and photonic devices, has progressed in the last few years as novel and unique properties are emerged, which may substantially be able to solve the complex existing problems in the domain of communication and information processing [1–3]. Owing to the synchronized development in material science and nano-fabrication technique [4, 5], in-depth investigations in both experimental and

theoretical ways on semiconductor nanostructures lead to the possible realization of novel electronic [6, 7] and photonic [8, 9] devices. Quantization of energy states in low-dimensional semiconductors along different directions leads to the formation of quantum well, wire or dot, which are characteristically different from their bulk counterparts. It would be very difficult today to imagine solid state physics without semiconductor heterostructures, more precisely double heterostructures. The genesis of semiconductor electronics is from the feasibility of conductivity tuning by external impurities by means of doping. This feature along with the concept of non-equilibrium carrier injection helps to breed the semiconductor industry. Heterostructures provide the potential means for solving the far more general problem of controlling fundamental parameters in semiconductor crystals and devices, such as the width of the bandgap, the effective masses and mobilities of charge carriers, the refractive index and the electron energy spectrum. These structures can be used as infrared detectors [10, 11], which has immense applications in medical [12], defense [13] and communication [14] fields. Characteristics of these IR devices may be studied from absorption coefficient profile, and thus its accurate determination becomes very important from device design point of view.

To understand the electronic and optical properties of the nanostructures, computation of their eigenstates is very essential along with density of states profile [15]. Among the quantum structures, quantum well is extensively researched in the last decade because of computational advantages [16–18] and also eases of fabrication [19]. Multiple quantum well structures are subject to theoretical and experimental research in last two decades because of the resonant tunneling phenomenon [20], and novel photonic devices are already designed as transmitter [21] and receiver [22] applicable in nanoelectronic domain. By virtue of quantum engineering, electronic energy states are tuned by suitable application of external excitation in this complex multilayered structure as per the requirement by tailoring the electronic and optoelectronic properties of quantum heterostructures. One such example is the THz laser design with low-dimensional semiconductor structures [23] with multiple layers, where miniband formation and its energy difference with lowest quantum energy state (lowermost energy band) play crucial factor in governing the device performance [21] as optical transmitter. This is one typical semiconductor laser with room temperature operation at IR range, with good peak output power and CW mode of operation [24]. Operation of this unipolar device is based on quantum tunneling and intraband transitions, and formation of miniband critically depends on layer dimensions, their compositions and periodicity [25]. The layer thickness is essentially responsible for determining the wavelength of emitted radiation, as compared to the other semiconductor-based lasers where bandgap of the material determines the wavelength. Thus, accurate determination of electronic band structure of quantum cascade laser (QCL) is very important for theoretical researchers from the point of view of optoelectronic application.

2. Literature review

Semiconductors form the basis for the most modern information processing devices. Electronic devices, such as diodes, bipolar junction transistors and field effect transistors, drive modern electronic technology. Optoelectronic devices, such as laser diodes, modulators and detectors,

http://dx.doi.org/10.5772/66942

drive the optical networks. In addition to devices, semiconductor structures have provided the stages for exploring questions of fundamental physics. Quantum Hall effect and other phenomena associated with many-body effects and low dimensions have been studied in semiconductor structures.

Theoretical and experimental researches are so far carried out on the abrupt semiconductor heterostructure composition, precisely the combination of GaAs and AlGaAs. The popularity of this material system is due to the fact of near-perfect match between the GaAs and AlAs binary components. Interestingly, bandgap of GaAs is not suitable for the application of IR detectors, optical transmitter design at infrared region, long-wavelength optical sources and signal processing devices. Several moderate and narrow gap materials are already emerged out for signal processing applications and also for sensing elements in electrical circuits. To name a few, InSb, InAs and GaSb are the materials on which researchers are conceded, and these are categorized as emerging narrow gap materials. Their acceptance of making quantum devices is primarily due to the higher mobilities, bandgaps correspond to the infrared region of electromagnetic spectrum, saturation drift velocities and very low effective mass. Combination of these properties provides higher quantum confinement energies. Higher eigenenergies lead to the possibility of exhibiting mesoscopic property, that is, Aharonov-Bohm effect and Coulomb Blockade effects at higher temperatures.

One of the most interesting research areas in the low-dimensional semiconductor heterostructure is to study novel electronic and photonic properties, which already initiate some technological revolutions [26]. Quantum well, wire and dot are the examples of nanostructure, where quantized dimension has the order of de-Broglie wavelength. Quantum well is the most popular one, can be coupled with external world by means of resonant tunneling. This phenomenon leads the various researches in the last two decade for low-bias applications. Freire [27] calculated multiple-quantum-well (MQW) laser parameters for a dispersion supported transmission system. At very high transmission speed (20 Gbit/s), optical system is simulated for laser parameters using multiple-quantum-well (MQW) system. For strained layer MQW laser, simulation parameters are precisely estimated through signal intensity modulation (IM) response model in order to obtain response curve for communication application. Recently, Taghavi [28] showed that transistor performance can be improved if isolated well is replaced multiple well system. Significant enhancement in device performances is anticipated when the MQW structure is properly designed. Stöhr et al. [29] experimentally characterized electro-optical modulators and switches based on MQW-structure. It can also be used for making quantum cascade laser (QCL) [30], resonant tunneling diode (RTD) [31], resonant tunneling transistor (RTT) [32], quantum well infrared photodetectors (QWIP) [33], etc., which have greater efficiency compared to their bulk counterparts. QCLs are preferred for broadband tuning, RTD and RTT for digital circuits and negative resistance devices. QWIP is used for night vision and medical diagnostics.

Transmission coefficient needs to be computed for analysis of quantum well structures, and also for studying tunneling probability by various numerical approaches like variational method [34], Airy's function approach [35, 36], finite element method [37], transfer matrix technique (TMT) [7, 38–40] and weighted potential method [41]. A comparative analysis among these methods reveals the fact that TMT is one of the best effective procedures. For multibarrier

structure analysis at biasing condition, a theoretical estimation about transmission coefficient [17, 38, 42–45] gives corresponding estimation of eigenstates. Significant theoretical contributions on quantum well multilayered heterostructures deal with resonant tunneling mechanism, which is obtained based on accurate solution of the Schrodinger equation subject to the application of uniform magnetic field or constant electric field applied along the perpendicular direction of confinement or along the direction of confinement. Adopting transfer matrix technique, the transmittivity of the multilayered structure is calculated with incident electron energy in the presence or absence external field. Simulated results show good agreement with other existing model, and also with bound-state energies. Based on these calculations, a new class of resonant tunneling superlattice devices has been designed.

Miller [46] investigated the effect of band nonparabolicity on eigenenergies using Kane's two-band model, later considered as a function of material parameters by Hiroshima [47]. Nonparabolicity is accounted for calculation of transmission coefficient by Palomino-Ovando [48]. He used transfer matrix technique (TMT) with nonparabolic dispersion relations for conduction band electrons, which is incorporated in the modified Schrödinger equation; and 2 × 2 matrices are generated. This method is implemented to the study of quasi-periodic semiconductor heterostructures maintaining Fibonacci series property. Miniband formation is observed and amplitudes of resonant tunneling peaks are measured. Results are compared with that obtained for parabolic case to justify the importance of nonparabolic deviations in $Al_xGa_{1-x}As$/GaAs superlattices.

Multiple quantum well structure is a low-dimensional semiconductor nanostructure which is coupled through the external world by means of resonant tunneling; and based on this physical insight, several novel electronic [31, 32] and photonic [30–33] devices are fabricated which is far superior to their bulk counterparts. The analysis of resonant tunneling diodes was carried out with submicron-sized mesa structures along with contacts at both the terminals in order to measure the current-voltage characteristics in the bistable regime at room temperature. Investigation reveals the noise-triggered firing of spike-like signals from the RTD's biased dynamically, and they act as universal logic gates with reconfigurable property for mini voltage changes ranging from a few mV at the input coordinates. It has also been shown that the RTD junction can be easily integrated to arrays of multiple inputs and has thus the potential to mimic neurons in nanoelectronic circuits.

RTD is already used with slot antenna. With an offset-fed slot antenna, the device is placed at a specified distance w.r.t. slot center, and used in oscillator with considerable output power (100–200 μW) at frequencies of 430–460 GHz. If the distance from the slot center is kept 45 μm for 100 μm long antenna, then 200 μW output power can be obtained (which was the maximum power) at 443 GHz for a single RTD device with a peak current density of 18 mA/μm^2. This opened the door of possible application of quantum well–based devices for communication application at both transmitting and receiving ends. Simultaneous optimization of antenna length and position of quantum device enhances the output performance. Based on this novel investigation and superior performance, a large-format (640 × 512) voltage-tunable quantum-well (QW) infrared photodetector focal plane array (FPA) is designed for both the mid- and long-wavelength infrared (MWIR and LWIR) bands for the sole purpose of imaging applications. Using MBE technique, 8 well MWIR stack with AlGaAs-InGaAs composition

and 16 well LWIR stack with AlGaAs-GaAs system are developed and series connection is made between them which provided excellent voltage-tunable spectral response property. Results show a very well redshift of peak responsivity (4.8–8.4 μm, within IR range) with increase of bias within the applicable limit as determined by commercial IC's.

Biasing effect on the lowest three eigenstate of four-barrier three-well MQW structure assuming realistic band structure has been studied by accounting conduction band nonparabolicity. Only first-order nonparabolic effect is considered, and transfer matrix technique is used to solve the problem. GaN/Al_xGa_{1-x} N material composition is assumed for simulation purpose, as the device is aimed to design optical transmitter. The method is well established [38, 39], and results obtained by using TMT are quite accurate when compared with the results obtained using other methods.

Semiconductor nanostructure is the topic of research in the last decade due to its possible novel applications in the field of electronics [9] and photonics [49]. It has been studied that the photonic crystals composed of at least two different semiconductor heterostructures exhibit resonant photonic states, and the composition may be termed photonic double quantum well (PDQW). The heterostructure is schematically denoted as ....Q/P/Q/P/Q...., where P and Q act as photonic wells and barriers depending on their refractive indices, and thus bandgaps, respectively. The resulting band structure exhibits photonic bandgap, similar to the electronic bandgap in semiconductor and dielectric, and photons having energy within that electromagnetic forbidden region could not propagate. This leads to the discrete quantized states. Mathematical modeling has already been carried out for the transmission coefficient of the PDQW heterostructure using both transfer matrix method and plane wave propagation method, and it has been found that within the photonic wells, resonant states exist in split pair mode. This is due to the fact that coupling between degenerate states due to the propagation of forward and backward waves inside this electromagnetic structure, resonant states originate, and it is shared by the both layers of the unit block. Simulation study reveals that resonant states appear as single peak in the transmission spectrum when the energy is within the range of bound photonic state, and then separation distance between the adjacent photonic quantum wells is very large. However, with reduction of the thickness of the sandwiched barrier layer, energy-splitting effect is observed, which is represented by two adjacent resonant peaks in the transmission profile. This realization makes the possible operation of the device as switch single and double transparent states. Similar to the electronic MQW system, in the photonic structure also, number of resonant states can be tailored by varying the dimension of the photonic wells and barriers. Also by increasing the contact barrier widths, quality factor of transmitted peaks can be significantly improved. Researchers are already performed to utilize this property in developing optical filter, transmitter, switch, quantum information processing, receiver and devices, which are suitable in all-optical integrated circuits. The major unique feature if these devices are they are pure photonic devices compared with the existing optoelectronic devices. Quantum confinement is made by reducing the device dimensions of the order of electron wavelength along one, two or three dimensions; results in quantum well, wire or dot, respectively. These quantum systems are usually coupled with the external world through tunneling barriers, which vividly reflect the dominance of the quantum effects to understand the physical properties of heterostructure devices; and the discrete electronic states become resonant one.

Calculation of these eigenstates thus becomes very essential to study the electronic and optoelectronic behavior of the nanodevices [50, 51]. For determining eigenstates, BenDaniel-Duke boundary condition is incorporated in order to consider the effect of effective mass mismatch at different hetero-interfaces, as well as to consider the conduction band discontinuity, which leads to the quantum well potential height. Difference of bandgap gives the second consideration, whereas numerical calculation reveals that results are erroneous when constant effective mass is considered. This signifies the effect of boundary condition at numerical estimation. Structural parameters (in terms of thicknesses of the layers and number of layers) are important players in tuning the energy values. Simulations are also performed in the presence and absence of electric field. In most of the literatures, GaAs/$Al_xGa_{1-x}As$ material composition is considered to understand tunneling probability.

Material compositions of the heterostructures also have a profound effect on the transmission characteristics under resonance condition. Among the quantum structures, quantum well is already studied a lot [16–52] because of computational advantages for analysis and also eases of fabrication [17, 53]. Density of states is one of the very important parameter of nanostructure as it provides the eigenstates from lowermost value [54]. Its profile is changed by application of external field; thus a comparative study my reveal the possibility of low-bias applications through resonant tunneling. Work on density of states of quantum well is carried out by researchers in presence of inelastic scattering [55] along with computation of transmission probabilities. It has been shown that shot noise in a resonant tunneling diode biased in the negative differential resistance regions of the I–V characteristic is enhanced with respect to 'full' shot noise. Experimental results suggests that profile of density of states function for particular type of quantum well system is the governing cause of the so-called noise effect, physically controlled by electron-electron interaction through Coulomb force. Numerical results are also presented from the above-mentioned theory, which are in close proximity with the experiment. This ensures that the model presented is accountable for the relevant physics involved in the phenomenon.

Step-like shape of the density of state (DOS) profile is used to study the characteristics of heterostructure well laser [56]. For finite-barrier quantum well, it differs from what obtained for infinite well problem [57]. The results presented in this chapter, obtained by applying the correspondence with the bulk density of states (DOS), indicate that the DOS in finite-barrier quantum wells differs substantially from the conventional 2D DOS calculated for infinite-barrier quantum wells.

Peak of the DOS is analytically related with the occurrence of resonance [58] along with transmission and reflection phase times. Existence of quasi-bound states is observed from DOS plot [59] for specially designed rectangular well structures. Numerical calculations have been presented, which substantially prove that electron states are present in the continuous part of the spectrum for different quantum well devices irrespective of well geometry. Initial works are carried out on rectangular potential profiles. Necessary boundary conditions for creation of these quasi-states are theoretically investigated. At very high energies in conduction band, existence of these quasi-bound states with spatial localization is determined. The results can be very useful in design of semiconductor optoelectronic devices whose working principle will be based on continuum bound states.

http://dx.doi.org/10.5772/66942

With the emergence of nanoelectronic devices as the possible replacement of existing VLSI technology, the need of resonant tunneling device in sub-micron domain becomes very important for low bias application point of view, and theoretical research for accurate design of these structures leads to the invention of novel electronic and optoelectronic properties. Ultrathin semiconductor quantum devices are now the interests of research where quantum well, wire and dot have already realizable because of the advancement of microelectronics technology. For accurate estimation of resonant tunneling, displacement of energy levels from the band-edge should be considered; hence, realistic band structure plays a very important role for different material parameters. This leads to the better computation of intersubband transition energy for optical emitter/detector design [50, 60]. Intersubband transition energy is computed for core-shell (normal and inverted) quantum dots (CSQD) of cubic and spherical geometries by solving time-independent Schrödinger equation using finite-difference technique. Sparse, structured Hamiltonian matrices of order $N^3 \times N^3$ for cubic and $N \times N$ for spherical dots are produced considering N discrete points in spatial direction. The matrices are diagonalized to obtain eigenstates for electrons. Computed results for the lowest three eigenstates and intersubband transitions are shown for different structural parameters taking GaAs/Al_xGa_{1-x}As-based CSQD as an example. Reduction of subband transition energy is observed with increase in core thickness. A comparative study reveals that spherical CSQD exhibits higher transition energy between any two subbands than that is demonstrated by cubic CSQD of similar dimension and equal material composition. More interesting phenomenon is observed for inverted core-shell structure. In this case, transition energy monotonically decreases for cubic dot, while it is increased for spherical dot with enhancement in core size. These devices are utilized as optical emitter/detector due to the wider range of tuning in intersubband transition through tailoring dot dimensions.

Miller investigated the effect of conduction band nonparabolicity on eigenstates using Kane's two band model. Hiroshima showed the importance of material parameters to evaluate the same. Nelson introduced the energy-dependent effective mass theory [61] following Ben-Daniel Duke boundary condition for precise estimation of carrier energies. Palomino-Ovando extended the analysis for superlattice structure [62] where energy was calculated form transmission coefficient peaks. The work of Li in determining the electron states in multilayer semiconductor quantum devices plays a significant role. He showed that finite element method can effectively be used for near accurate determination of these electron states. Moreover, he emphasized on the importance of band structure consideration and showed the effect of Kane type conduction band nonparabolicity over the carrier states. For two different material compositions, the result is presented in tabular form.

This work is incorporated in modulator design [63]. Using multiple quantum well structures, authors show that spatial light modulators can be designed. Reflectance levels are calculated for 128 × 128 pixels ternary spatial light modulators with 10 KHz operating frequency. It is shown that single reflectance level can be duo with just a 180° phase difference. Structural design parameters of the modulator will play important role in determining the performance of the device.

Due to the rapid advancement in microelectronics technology [64, 65] in the last decade, research in the domain of semiconductor nanostructure has been carried out to a great extent by both theoretical [4, 66] and experimental workers [5, 6]. Quantum well waveguide is fabricated by ion implantation technique using InGaAsP/InP material composition. Multilayer structure is developed for waveguide gratings precisely for the application at CWDM wavelengths. Reactive ion etching technique is utilized to reduce the roughness below 5 nm (experimental results show surface roughness is approximately 2–3 nm). Significant findings emphasize the importance of this quantum device as cross talk between adjacent channels goes below −10 dB level in the transmission spectra of the waveguide. Moreover, insertion loss of the grating becomes less than 5 dB, which is another major advantage for communication application.

Heterostructure light emitting diode is made by InGaN/GaN composition using MOCVD technology. Strucutre is developed over $LiAlO_2$ (100) substrates consisting of multiple quantum well with five wells along with GaN p-n junction. Colors of the output emission (generally blue or green) depend on the indium composition of InGaN layer of the MQW structure. Proof of quantum well interface is experimentally obtained by third-order satellite peaks. These are measured by high resolution x-ray diffraction set-up. Good performances are reported in various literatures; for example, 3 mW output power is achieved for 800 × 800 μm^2 blue LED device with 200 mA input current. It is also experimentally observed that for green and blue LED's with InGaN/GaN composition, electroluminescence (EL) spectra suggest that peak wavelength almost saturates at some precise positions of the spectrum with enhancement of injection current. Henceforth, it may very easily be concluded that polarization fields are totally absent in the active region of the structure.

Spin-photonic semiconductor devices are the another novel class of quantum well based devices, which are researched in recent days due to the ability of controlling electronic and optoelectronic properties using the spin of conduction electrons. The two most promising examples of these devices are spin-switches and spin-vertical-cavity surface-emitting lasers (spin-VCSELs). Experimental investigation showed that circularly polarized laser with very high degree of circular polarization (0.96) at room temperature is obtained using GaAs/AlGaAs multiple quantum well vertical cavity surface emitting laser structure where spin relaxation time is very high (0.7 ns). Furhter works with the same structure also showed that carrier lifetime and electron spin relaxation time can be tuned by design parameters. This also modifies the lasing characteristic. Orientation of the wafer plane plays a very crucial role in this regard. All the experimental results are obtained for <110> wafer. Investigation is also conducted on p-i-n structure with similar material composition. Result showed that remarkable reduction of spin relaxation time can be obtained (4–0.3 ns) when the quantum well structure is subjected under external electric field applied along the direction of well width at room temperature. To understand the electronic and optical properties of the nanostructures, computation of their eigenstates is very essential along with density of states profile [16]. Among the quantum structures, quantum well is extensively researched in the last decade because of computational advantages [7, 8, 67] and also eases of fabrication [9].

Transfer matrix technique (TMT) and propagation matrix method (PMM) are the two most suitable cost-effective methodologies for the analysis of wave function profile, confined energy states and transmission coefficients in superlattice nanostructures. There are other numerical

methods like finite element method (FEM), finite difference method (FDM) but the complexity of the programming makes the computational time larger. However, these later methods are very accurate regarding the precision of the obtained results. Material composition for the ternary or quaternary heterostructures plays the bigger role along with Ben-Daniel Duke boundary conditions for determining the basic electrical properties of multilayered structures. Structural parameters within fabrication limit showed the variation of electronic (eigenenrgy, density of states, for example) and optoelectronic (absorption coefficient, oscillator strength, for example) properties of this superlattice structure which are pivotal in analysis of further complex structures. Otherwise multiple quantum well structures become a superlattice structure when width of the barrier layer between adjacent quantum wells is reduced to very small dimension, and this ensures the beginning of resonant tunneling through intermixing of the wavefunctions between the quantum wells. This provides a new insight in the nature of interacting wave functions for thin barriers. Number of wells in this computation becomes also important along with the structural parameters and material compositions. Different iterative methods are implemented for complex geometrical structures. Doping of the wells is taken into account through self-consistent solution of Schrödinger and Poisson's equations.

Thus, a comprehensive analysis of electronic and optical properties of MQW structures will make the foundation for understanding the quantum cascade laser. Its principle of operation is essentially dependent on the band structure, layer thickness is primarily responsible for determining the wavelength of emitted radiation, as compared to the other semiconductor based lasers where bandgap of the material determines the wavelength. Thus accurate determination of electronic band structure of quantum cascade laser is very important for theoretical researchers from the point of view of optoelectronic application.

3. Transmission coefficient of multiple quantum well structure

For analyzing electrical property of MQW structure, first transmission coefficient is calculated by considering a three-well four-barrier structure with rectangular potential profile configuration having GaN as well layer and $Al_xGa_{1-x}N$ as barrier layer. It is observed that by increasing well width, transmission probability increases. This is due to the fact that by increasing tunneling dimension of the well, quantum confinement decreases, so transmission can be achieved at lower energy values. By changing the material composition of barrier material, it is observed that transmission coefficient decreases with increase of Al mole fraction. It is plotted in **Figure 1**. This is due to the fact that by increasing Al percentage, potential height increases and effective mass mismatch at the junction also increases. This increases quantum confinement, which increases the eigenenergy. By increasing the thickness of the contact barrier, transmission probability reduces, whereas it increases if contact barrier thickness is reduced compared to that of the internal barriers. This is shown in **Figure 2** for both parabolic and nonparabolic band structures. By increasing number of wells, it is observed the eigenvalue reduces, and ultimately becomes constant for higher numbers, as evident from **Figure 3**. Eigenvalue increases with increase of material composition, as suggested from previous results, plotted in **Figure 4**. Obviously, for nonparabolic band structure, eigenenergy is less compared to the ideal parabolic concept. The variation is almost linear, and the gap reduces with increase of al mole fraction.

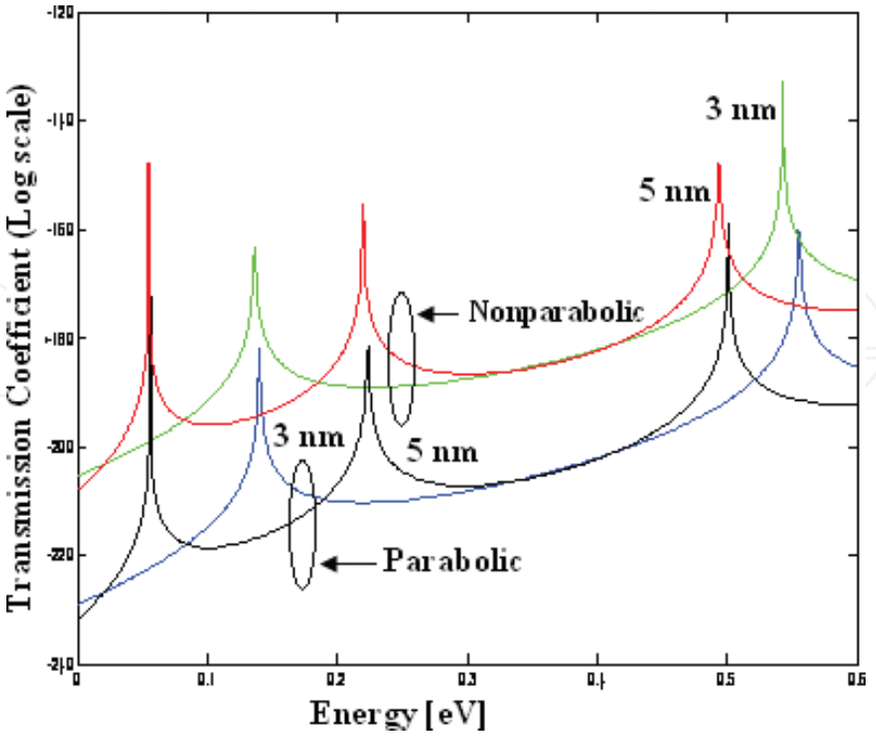

Figure 1. Transmission coefficient with energy for different barrier material composition for both parabolic and nonparabolic structure.

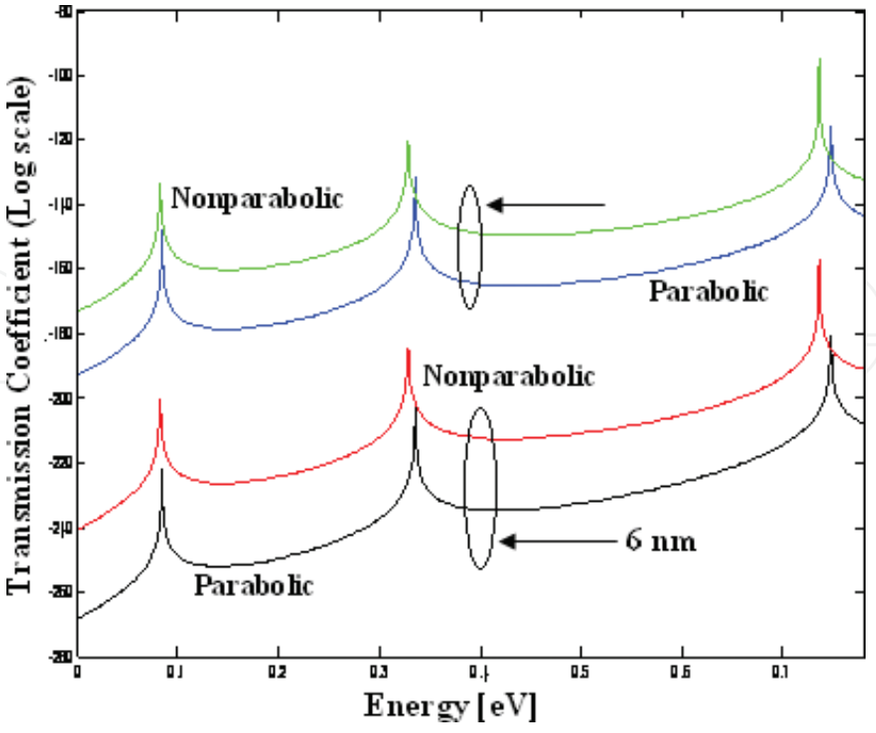

Figure 2. Transmission coefficient with energy for asymmetric barrier width for both parabolic and nonparabolic structure.

http://dx.doi.org/10.5772/66942

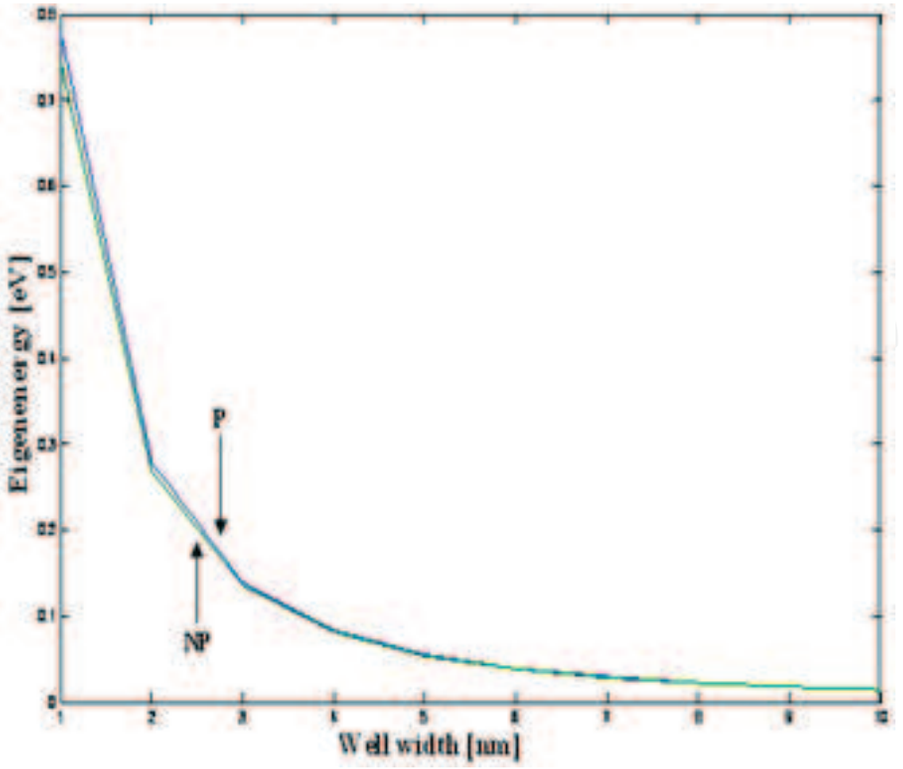

Figure 3. Eigen energy with dimension of well for both parabolic and nonparabolic structure.

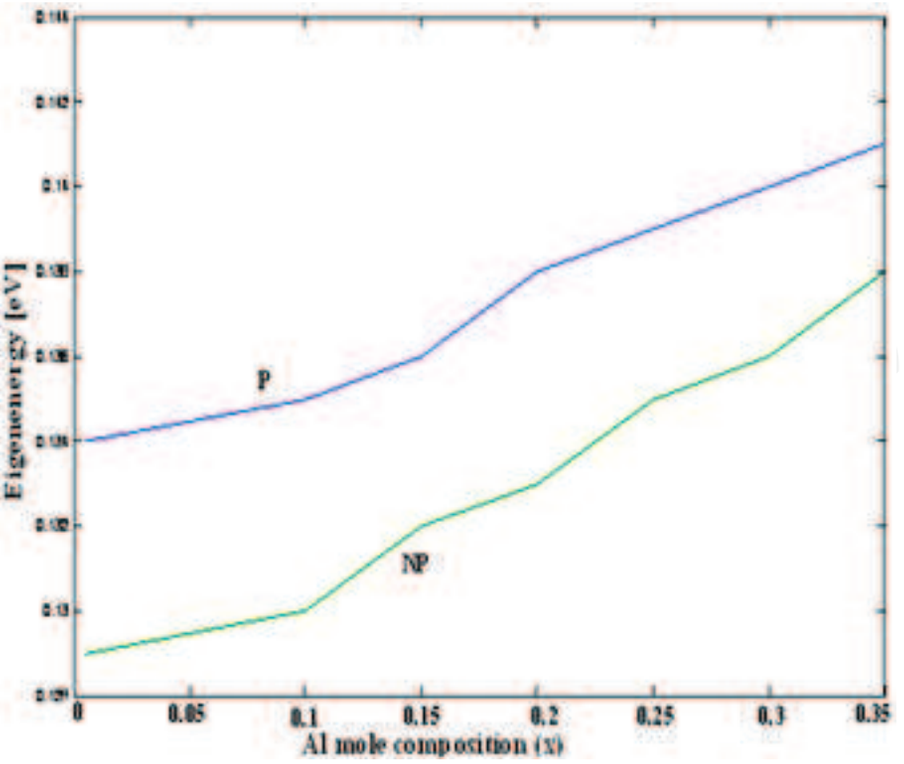

Figure 4. Eigen energy with barrier material composition for both parabolic and nonparabolic structure.

4. Density of states of MQW structure

In **Figure 5**, density of states (DOS) is plotted for lowest two eigenstates with different well widths. It is observed from the plot that by increasing the well width, eigenenergy appears at lower energy values due to the reduction of quantum confinement. It may also be seen that higher bandgap system provides eigenstate at lower energy range. Hence, optical device based on GaN/AlGaN system can be tuned at lower bias. Also due to closeness of first two energy levels in this composition, intersubband transition energy is higher for InAs/GaInAs system, which makes it efficient candidate for high frequency laser.

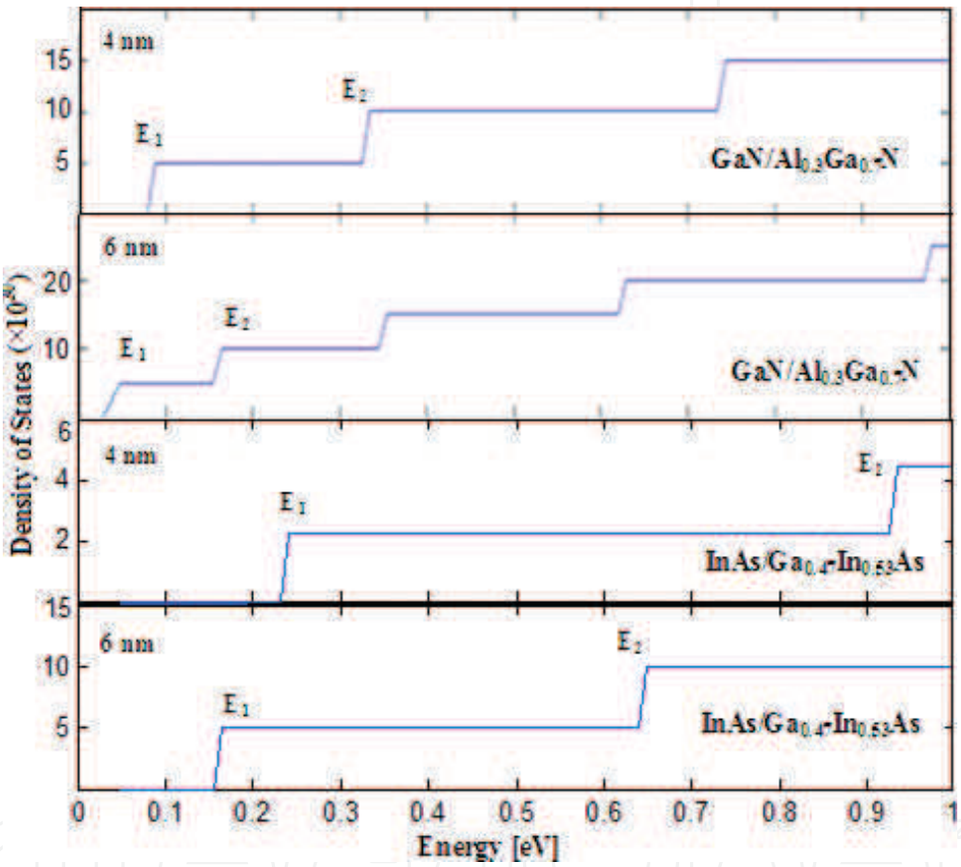

Figure 5. Density of states for the lowest two eigenstates for different well widths and different material compositions with nonparabolic dispersion relation.

Figure 6 shows the comparative study of DOS in presence and absence of electric field for InAs/GaInAs material composition. From the graph, it may be noted that application of transverse field lowers the magnitude of eigenstates irrespective of dispersion relation considered for simulation. Results are also compared with overestimated parabolic assumption. It may be observed from the comparison that incorporation of band nonparabolicity reduces the eigenvalue. Hence, for fine wavelength tuning purpose to design photonic transmitter/detector, realistic band structure consideration plays a vital role.

http://dx.doi.org/10.5772/66942

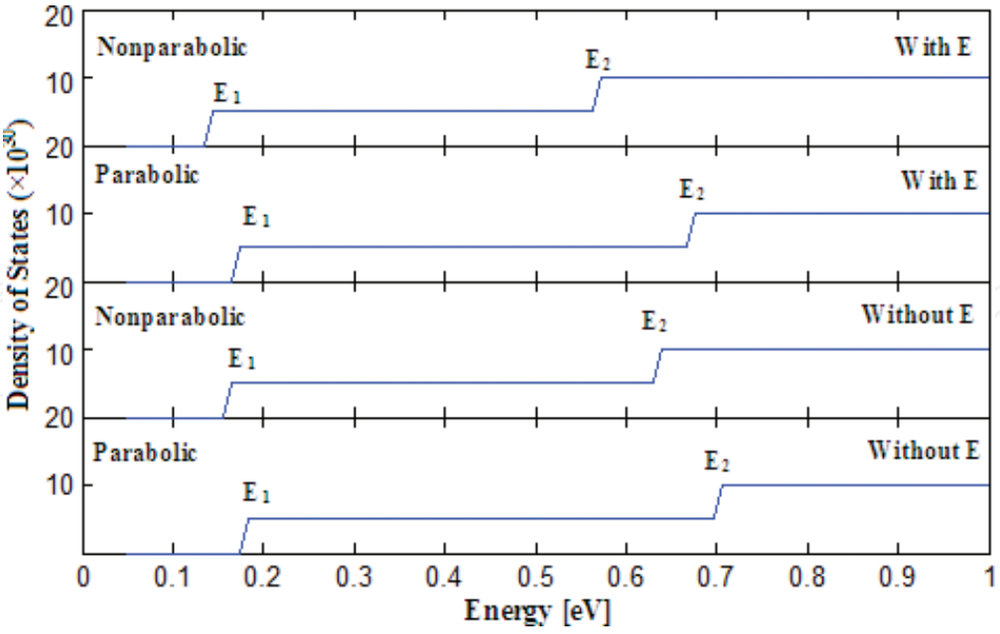

Figure 6. Density of States for the lowest two eigenstates in presence of absence of electric field for nonparabolic and parabolic structures.

By varying the material composition of barrier layers, it is observed that quantum states appear in higher energy values with increase of GaN mole fraction. The result is shown in **Figure 7**. This is because with increase of *x*, mismatch of effective mass increases as well as the conduction band discontinuity. This enhances the quantum confinement. Hence, eigenenergy increases. This is reflected via density of states plot.

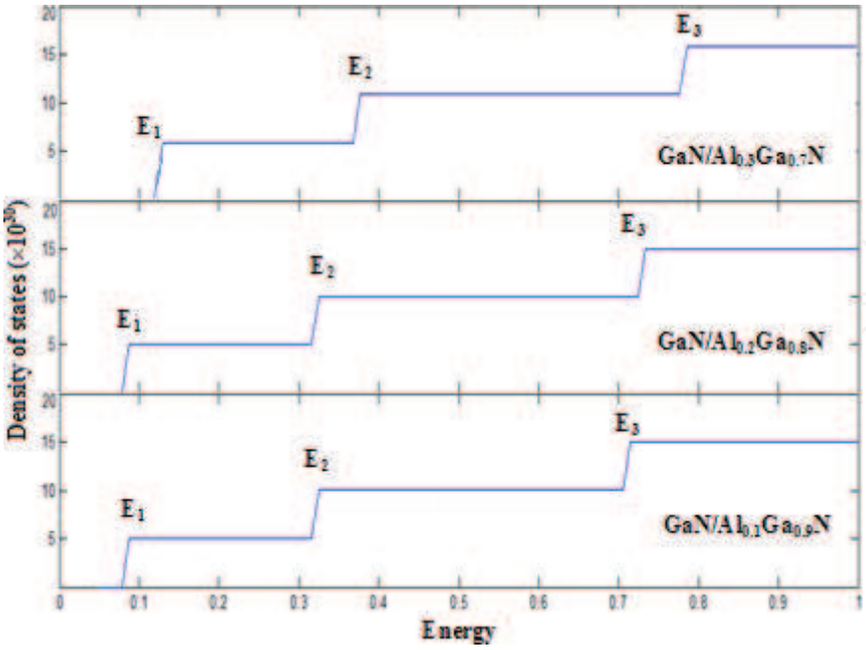

Figure 7. DOS of superlattice with different material compositions in absence of field considering band nonparabolicity.

5. Absorption coefficient of MQW structure

Absorption coefficient is calculated as a function of operating wavelength for different well width, as shown in **Figure 8**. For lower well dimension, it is found that the absorption coefficient value is less compared to the higher well dimension. Again, when the energy difference between the bands increases, interband transition energy increases. This reduces the peak of absorbance amplitude, provided half-width at half-maximum is kept constant throughout the simulation.

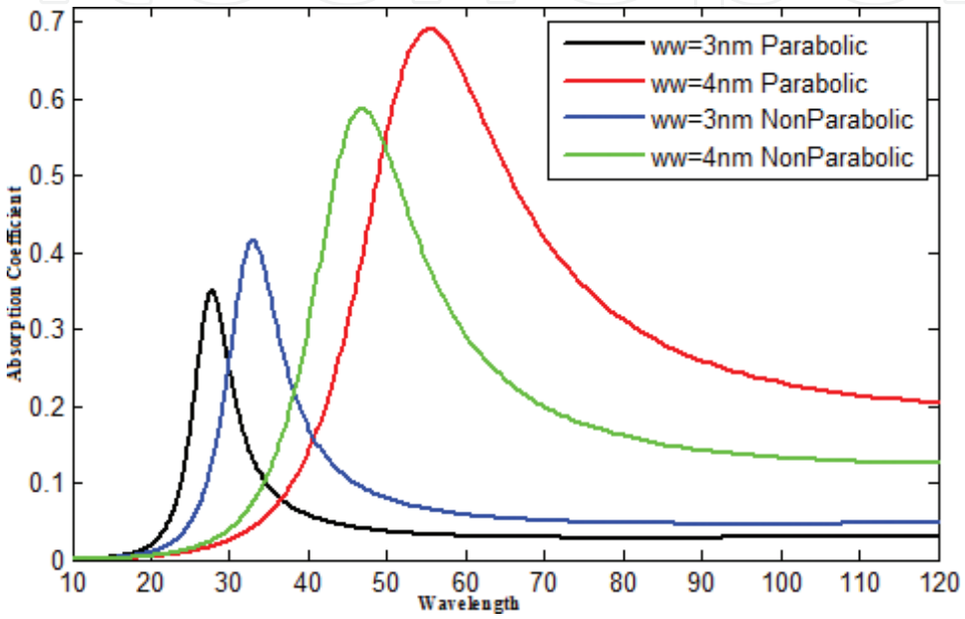

Figure 8. Absorption coefficient for different well dimension with wavelength variation for parabolic, nonparabolic dispersion.

With increase of well dimension, redshift is observed for all the profiles corresponding to the transition energies; also peak value is shifted rightwards and the wavelength value increases. When the parabolic and nonparabolic dispersion relation is considered for same well dimension the peak value is greater for lower well dimension nonparabolic case. But with change in eigenenergy, for higher well dimension the parabolic relation gives a higher absorption peak value. Thus the nonparabolic dispersion relation takes the priority for simulation.

With parabolic and nonparabolic relations into consideration the material composition is varied in accordance with the wavelength. The absorption coefficient profiles are depicted in **Figure 9**. For parabolic dispersion, the transition energies are low, so the absorption peak values are less compared to that of nonparabolic case. Also for higher material composition the shift in absorption value is considerable. The peak absorption values are greater for higher material composition and also for nonparabolic dispersion.

http://dx.doi.org/10.5772/66942

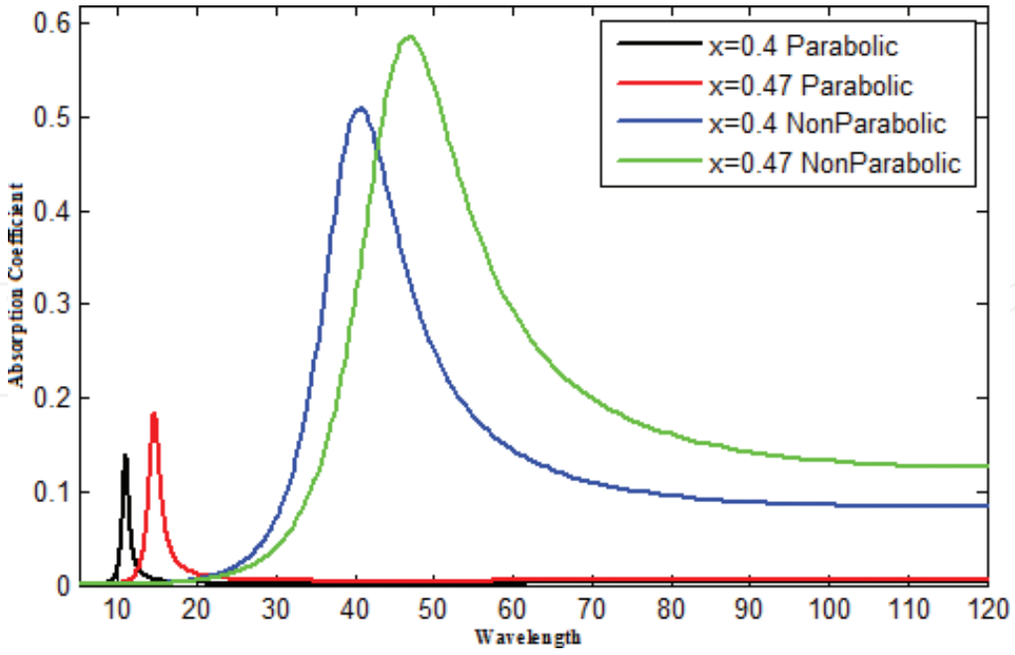

Figure 9. Absorption coefficient for different material composition with wavelength variation for nonparabolic and parabolic dispersion.

6. Band structure of quantum cascade laser

Electronic band structure of quantum cascade laser is analytically computed in presence of electric field applied along the direction of quantum confinement. At first, electronic and optoelectronic properties of the MQW structure is calculated. Next, miniband formation is observed for quantum cascade laser for a few precise magnitudes of electric fields. Separation of the miniband w.r.t. lowest energy band is calculated [68]. $Al_xGa_{1-x}As/GaAs$ composition is taken into account with the incorporation of Ben-Daniel Duke boundary conditions at hetero-interfaces. Eigenstates are calculated in presence and absence of Kane-type first-order conduction band nonparabolicity. Its variation as a function of applied field is determined, and is compared with the findings of zero bias conditions.

Figures 10–12 represent the electronic band structure of quantum cascade laser. For biasing, electric field is applied along the direction of quantum confinement, and eigenstates are computed. Results are also obtained when field is absent. While designing the structure, the most important aspect is that a distinguishable separation between injector and active region should be kept along with the miniband formation [68]. **Figure 10** shows the band diagram when external field is totally absent, and **Figure 11** demonstrated it for very high electric field (56.8×10^5 V/m). Here it may be noted that all the high magnitudes of electric field will not provide desirable QCL operation, as discrete miniband formation is necessary for that purpose. From the simulated observations, it may be indicated that the eigenenergy states are totally discrete in absence of external excitation, which are nothing but the eigenstates of a simple multiple quantum-well (MQW) structure.

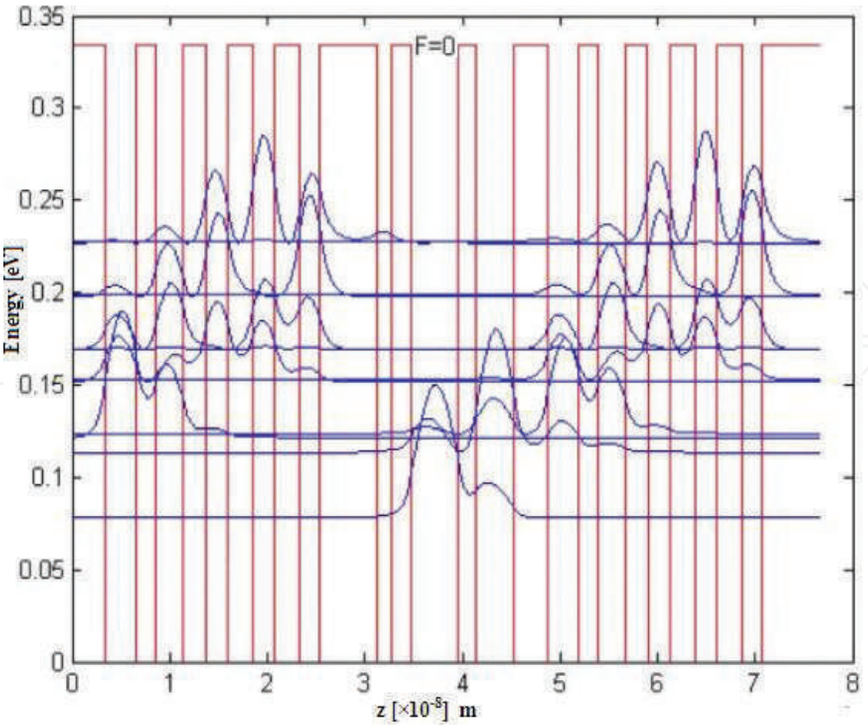

Figure 10. Electronic band structure of QCL without external bias.

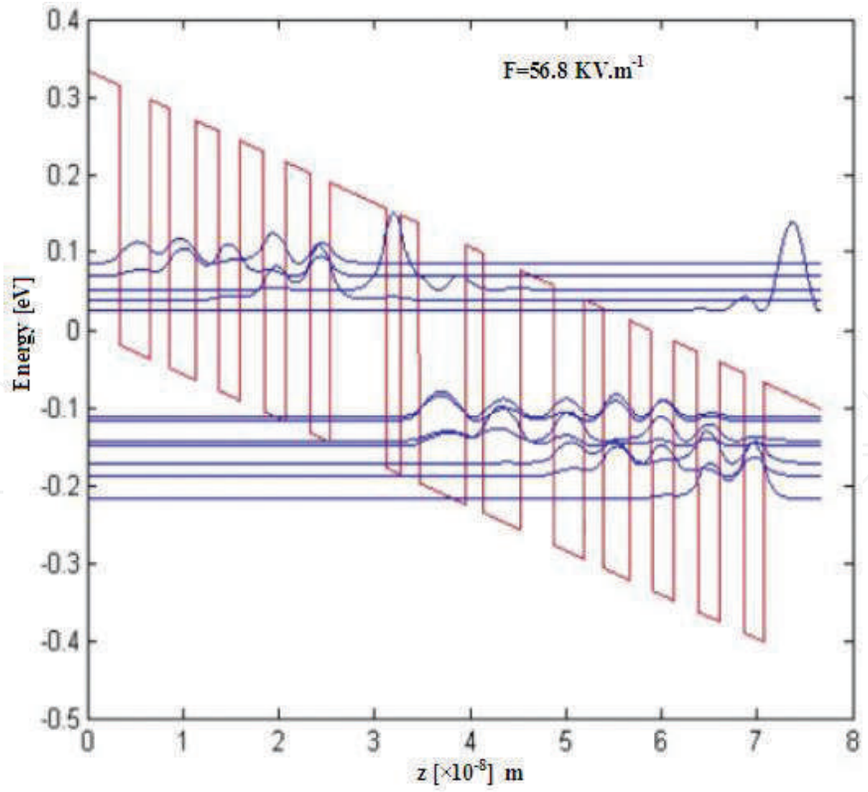

Figure 11. Electronic band structure of QCL with 56.8×10^5 V/m.

From **Figure 11**, it is observed that after application of very high electric field, miniband is formed over the ground state energy band. In this context, it may be noted down that after the injector region, active region starts, and the wavefunction starts to produce minibands. The energy gap between miniband and ground state energy band is distinguishable, which ensures the QCL operation. In this context, it may be pointed out that the magnitude of external field is chosen based on the structural dimensions and the material composition taken for the simulation. The structure is titled compared to **Figure 10**, along the direction of electric bias. Thus, the periodic growth of wavefunction in the miniband appears outside the confinement region, that is, in the quasi-continuous region. This band structure modulation is absent if the field is moderate (35.8×10^5 V/m).

Further reduction of electric field makes position of the miniband almost inside the confinement region, that is, miniband position is below the quasi-continuous region. This is shown in **Figure 12**. Eigenenergy variation with the applied bias for the laser is shown in **Figure 13**. Simulation result suggests that with increase of applied field, eigenenergy increases monotonically, and the rate reduces once filed crosses the value 35×10^5 V/m. Thus, stimulated emission between the miniband and the ground state energy band is effectively controlled by external bias.

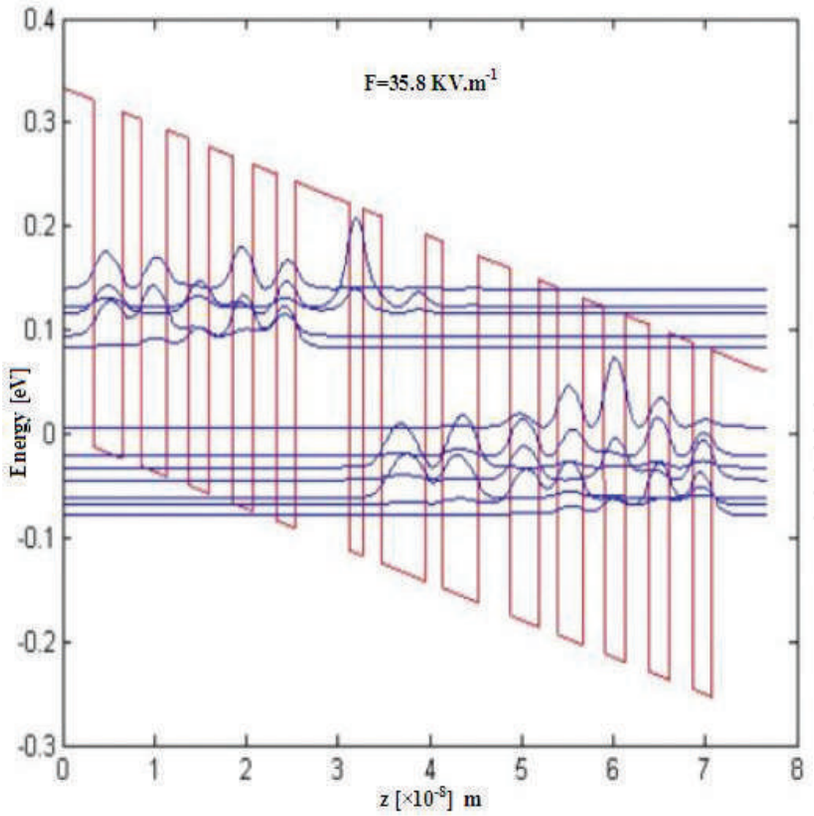

Figure 12. Electronic band structure of QCL with 35.8×10^5 V/m.

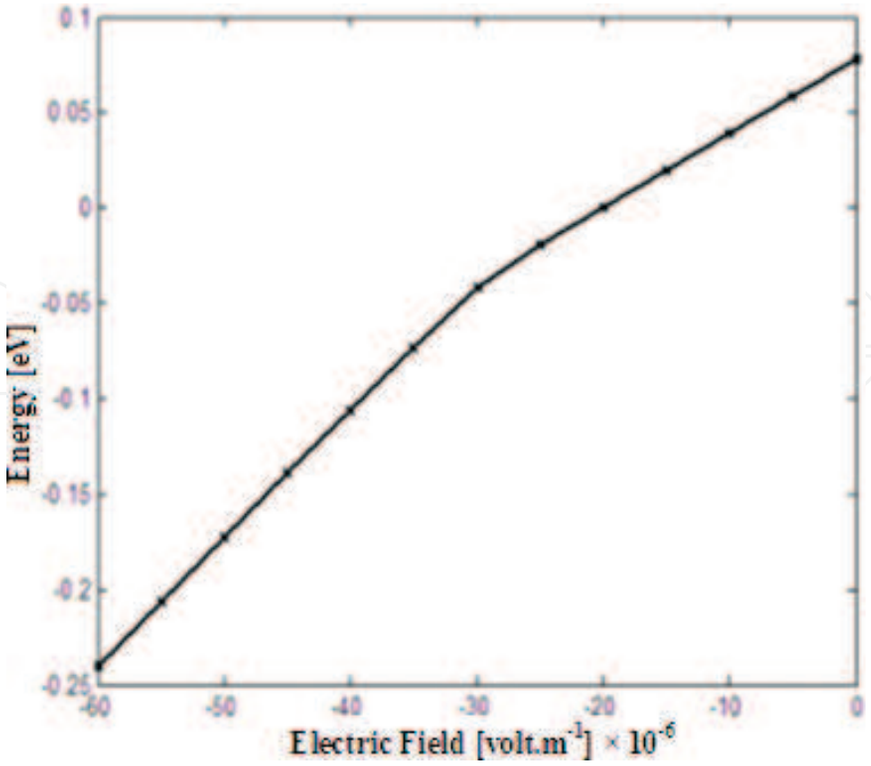

Figure 13. Variation of eigenenergy with applied field.

7. Conclusion

In this article, a detailed investigation on electrical and optoelectronic properties of multiple quantum well structure is carried out. Based on that structure, wavefunction in a quantum cascade laser at various biased conditions is analytically calculated and also for unbiased condition. It is proven and shown that miniband formation is only possible at some precise electric field. The method showed can also be applicable for the other structures. Key factor in this calculation is that position-dependent effective mass is considered for the simulation.

Author details

Arpan Deyasi

Address all correspondence to: deyasi_arpan@yahoo.co.in

Department of Electronics and Communication Engineering, RCC Institute of Information Technology, Kolkata, India

http://dx.doi.org/10.5772/66942

References

[1] Basu P K, Ghosh S, Mukhopadhyay B, Sen G: Ge/SiGeSn multiple quantum well photonic devices. 2nd National Workshop on Advanced Optoelectronic Materials and Devices. US, 2008.

[2] Fara S, Sterian P, Fara L, Iancu M, Sterian A: New results in optical modeling of quantum well solar cells. International Journal of Photoenergy. 2012, 2012:810801.

[3] Friel I, Thomidis C, Moustakasa T D: Ultraviolet electroabsorption modulator based on AlGaN/GaN multiple quantum wells. Journal of Applied Physics. 2005, 97:123515.

[4] Zhong S, Qu X: Design and fabricate InGaAlAs quantum well device for future optoelectronic integration. Advanced Materials Research. 2012, 442:188–192.

[5] Liu B, Han P, Xie Z, Zhang R, Liu C, Xiu X, Hua X, Lu H, Chen P, Zheng Y, Zhou S: Fabrication of blue and green non-polar InGaN/GaN multiple quantum well light-emitting diodes on LiAlO2(100) substrates. Physica Status Solidi(a). 2010, 207:1404–1406.

[6] Kuo Y, Lee Y K, Ge Y, Ren S, Roth J E, Kamins T E, Miller D A B, Harris J S: Strong quantum-confined Stark effect in germanium quantum-well structures on silicon. Nature. 2005, 437:1334–1336.

[7] Samuel E P, Patil D S: Analysis of wavefunction distribution in quantum well biased laser diode using transfer matrix method. Progress in Electromagnetics Research Letters. 2008, 1:119–128.

[8] Hitoshi K: Spin-photonic semiconductor devices based on (110) quantum wells: Spin-VCSELs and spin-switches. 13th International Conference on Transparent Optical Networks. IEEE. 2011, 1–4.

[9] Joel D, Singh M R: Resonant tunneling in photonic double quantum well heterostructures. Nanoscale Research Letters. 2010, 5:484–488.

[10] Yu C H, Zhang B, Lu W, Shen S C, Liu H C, Fang Y Y, Dai J N, Chen C Q: Strong enhancement of terahertz response in GaAs/AlGaAs quantum well photodetector by magnetic field. Applied Physics Letters. 2010, 97:022102.

[11] Kalchmair S, Detz H, Cole G D, Andrews A M, Klang P, Nobile M, Gansch R, Ostermaier C, Schrenk W, Strasser G: Photonic crystal slab quantum well infrared photodetector. Applied Physics Letters. 2011, 98:011105.

[12] Perera A G U: Quantum structures for multiband photon detection. Opto-Electronics Review. 2006, 14:103–112.

[13] Phillips M C, Taubman M S, Bernacki B E: Design and performance of a sensor system for detection of multiple chemicals using an external cavity quantum cascade laser. Proceedings of SPIE. 2010, 7608:76080D.

[14] Wei R, Deng N, Wang M, Zhang S, Chen P, Liu L, Zhang J: Study of Self-assembled Ge Quantum Dot Infrared Photodetectors. 1st IEEE International Conference on Nano/Micro Engineered and Molecular Systems. US, 2006, 330–333.

[15] Harrison P: Quantum Wells, Wires and Dots: Theoretical and Computational Physics of Semiconductor Nanostructures, John Wiley, New York, 4th edition, 2016.

[16] Talele K, Patil D S: Analysis of wave function, energy and transmission coefficients in GaN/AlGaN superlattice nanostructures. Progress in Electromagnetics Research. 2008, 81:237–252.

[17] Simion C E, Ciucu C I: Triple-barrier resonant tunneling: A transfer matrix approach. Romanian Reports in Physics. 2007, 59:805–817.

[18] Kundu P, Ghosh P, Deyasi A: Analytical computation of absorption coefficient for intersubband transition in MQW structure. Lecture Notes in Electrical Engineering: Computational Advancement in Communication Circuits and Systems [SPRINGER], part 6. Advances in Devices and Circuit. 2014, chapter 35, 335:321–329.

[19] Andrew S R, Marsh J H, Holland M C, Kean A H: Quantum well laser with integrated passive waveguide fabricated by neutral impurity disordering. IEEE Photonics Technology Letters. 1992, 4:426–428.

[20] Kubis T, Mehrotra S R, Klimeck G: Design concepts of terahertz quantum cascade lasers: Proposal for terahertz laser efficiency improvements. Applied Physics Letters. 2010, 97:261106.

[21] Cooper J D, Valavanis A, Ikonic Z, Harrison P, Cunningham J E: Finite difference method for solving the Schrödinger equation with band nonparabolicity in mid-infrared quantum cascade lasers. Journal of Applied Physics. 2010, 108:113109.

[22] Lin S H, Feng D J Y, Lee M L, Lay T S, Sun T P, Kuan C: Double-barrier superlattice infrared photodetector integrated with multiple quantum-well infrared photodetector to improve performance. International Journal of Electrochemical Science. 2012, 7:5746–5753.

[23] Razavipour S G, Dupont E, Chan C W I, Xu C, Wasilewski Z R, Laframboise S R, Hu Q, Ban D: A high carrier injection terahertz quantum cascade laser based on indirectly pumped scheme. Applied Physics Letters. 2014, 104:041111.

[24] Bugajski M, Kosiel K, Szerling A, Karbownik P, Pierściński K, Pierścińska D, Hałdaś G, Kolek A: High performance GaAs/AlGaAs quantum cascade lasers: Optimization of electrical and thermal properties. Proceedings of SPIE. 2012, 8432:84320I.

[25] Yamamoto H: Resonant tunneling condition and transmission coefficient in a symmetrical one-dimensional rectangular double-barrier system. Applied Physics A: Materials Science & Processing. 1987, 42:245–248.

[26] ITRS: Roadmap, http://www.itrs2.net/itrs-reports.html, 2007.

[27] Freire M, Silva H J A: Estimation of multiple-quantum well laser parameters for simulation of dispersion supported transmission systems at 20 Gbit/s. IEE Proceedings-Optoelectronics. 1999, 146:93–98.

[28] Taghavi I, Kaatuzian H, Leburton J P: Multiple versus single quantum well transistor laser performances. Integrated Photonics Research, Silicon and Nanophotonics. US, 2012, IM4B: IM4B.5

[29] Stöhr A, Humbach O, Zumkley S, Wingen G, David G, Jäger D, Bollig B, Larkins E C, Ralston J D: InGaAs/GaAs multiple-quantum-well modulators and switches. Optical and Quantum Electronics. 1993, 25:S865–S883.

[30] Fujita K, Edamura T, Furuta S, Yamanishi M: High-performance, homogeneous broad-gain quantum cascade lasers based on dual-upper-state design. Applied Physics Letters. 2010, 96:241107.

[31] Worschech L, Hartmann F, Kim T Y, Ho-fling S, Kamp M, Forchel A, Ahopelto J, Neri I, Dari A, Gammaitoni L: Universal and reconfigurable logic gates in a compact three-terminal resonant tunneling diode. Applied Physics Letters. 2010, 96:042112.

[32] Hinata K, Shiraishi M, Suzuki S, Asada M, Sugiyama H, Yokoyama H: Sub-terahertz resonant tunneling diode oscillators with high output power (200 μw) using offset-fed slot antenna and high current density. Applied Physics Express. 2010, 3:014001.

[33] Eker S U, Kaldirim M, Arslan Y, Besikci C: Large-format voltage-tunable dual-band quantum-well infrared photodetector focal plane array for third-generation thermal imagers. IEEE Electron Device Letters. 2008, 29:1121–1123.

[34] Bastard G, Mendez E E, Chang L L, Esaki L: Variational calculations on a quantum well in an electric field. Physical Review B. 1983, 28:3241–3245.

[35] Ghatak A K, Thyagarajan K, Shenoy M R: A novel numerical technique for solving the one-dimensional Schrödinger equation using matrix approach—application to quantum well structures. IEEE Journal of Quantum Electronics. 1988, 24:1524–1531.

[36] Brennan K F, Summers C J: Theory of resonant tunneling in a variably spaced multi-quantum well structure: An airy function approach. Journal of Applied Physics. 1987, 61:614–623.

[37] Hayata K, Koshiba M, Nakamura K, Shimizu A: Eigenstate calculations of quantum well structures using finite elements. Electronics Letters. 1988, 24:614–616.

[38] Sugg A R, Leburton J P C: Modeling of modulation-doped multiple-quantum-well structures in applied electric fields using the transfer-matrix technique. IEEE Journal of Quantum Electronics. 1991, 27:224–231.

[39] Jonsson B, Eng S T: Solving the Schrödinger equation in arbitrary quantum-well profiles using the transfer-matrix method. IEEE Journal of Quantum Electronics. 1990, 26:11.

[40] Hong Y J, Zhi J G, Yan Z, Wu L W, Chun S Y, Guo W Z, Jun X J: Resonant tunneling in barrier-in-well and well-in-well structures. Chinese Physics Letters. 2008, 25:4391–4394.

[41] Tsuji Y, Koshiba M: Analysis of complex eigenenergies of an electron in two- and three-dimensionally confined systems using the weighted potential method. Microelectronics Journal. 1999, 30:1001–1006.

[42] Austin E J, Jaros M: Electronic structure of an isolated GaAs-GaAlAs quantum well in a strong electric field. Physical Review B. 1985, 31:5569–5572.

[43] Harwit A, Harris J S: Calculated quasi-eigenstates and quasi-eigenenergies of quantum well superlattices in an applied field. Journal of Applied Physics. 1986, 60:3211–3213.

[44] Guoa Y, Gu B L, Yu J Z, Zeng Z, Kawazoe Y: Resonant tunneling in step-barrier structures under an applied electric field. Journal of Applied Physics. 1988, 84:918–924.

[45] Allen S S, Richardson S L: Theoretical investigations of resonant tunneling in asymmetric multibarrier semiconductor heterostructures in an applied constant electric field. Physical Review B. 1994, 50:11693–11700.

[46] Miller R C, Kleinman D A, Gossard A C: Energy-gap discontinuities and effective masses for GaAs-$Al_xGa_{1-x}As$ quantum wells. Physical Review B. 1984, 29:7085–7087.

[47] Hiroshima T, Lang R: Effect of conduction-band nonparabolicity on quantized energy levels of a quantum well. Applied Physics Letters. 1986, 49:456–457.

[48] Palomino-Ovando M, Cocoletzi G H, Perez-Lopez C: Band nonparabolicity in quasi-periodic Fibonacci heterostructures. Physics Letters A. 1996, 213:191–196.

[49] Chanda A, Eastman L F: Quantum mechanical reflection at triangular planar-doped potential barriers for transistors. Journal of Applied Physics. 1982, 53:9165–9169.

[50] Deyasi A, Bhattacharyya S, Das N R: Computation of intersubband transition energy in normal and inverted core-shell quantum dots using finite difference technique. Superlattices & Microstructures. 2013, 60:414–425.

[51] Deyasi A, Bhattacharyya S, Das N R: A finite difference technique for computation of electron states in core-shell quantum wires of different configurations. Physica Scripta. 2014, 89:065804.

[52] Esaki L, Chang L L: New transport phenomenon in a semiconductor superlattice. Physical Review Letters. 1974, 33:495–498.

[53] Tsukamoto S, Nagamune Y, Nishioka M, Arakawa Y: Fabrication of GaAs quantum wires on epitaxially grown V grooves by metal-organic chemical-vapor deposition. Journal of Applied Physics. 1992, 71:533–535.

[54] Arakawa Y, Nagamune Y, Nishioka M, Tsukamoto S: Fabrication and optical properties of GaAs quantum wires and dots by MOCVD selective growth. Semiconductor Science and Technology. 1993, 8:1082–1088.

[55] Khalil H M, Balkan N: Carrier trapping and escape times in p-i-n GaInNAs MQW structures. Nanoscale Research Letters. 2014, 9:21.

[56] Iannaccone G, Pellegrini B: Compact formula for the density of states in a quantum well. Physical Review B. 1996, 53:2020–2025.

[57] Holonyak N, Kolbas R M, Dupuis R D, Dapkus P D: Quantum-well heterostructure lasers. IEEE Journal of Quantum Electronics. 1980, 16:170–186.

[58] Osinski M, Mojahedie M: Density of confined states in finite-barrier quantum wells. LEOS '93 Conference Proceedings. IEEE. 1993, 635–636.

[59] Carrillo-Delgado E A, Rodriguez-Vargas I, Vlaev S J: Continuum electronic bound states in rectangular quantum wells and barriers. PIERS. 2009, 5:137–140.

[60] Deyasi A, Bhattacharyya S: Interband transition energy of circular quantum dots under transverse magnetic field. Physics Procedia. 2014, 54:118–126.

[61] Nelson D F, Miller R C, Kleinman D A: Band nonparabolicity effects in semiconductor quantum wells. Physical Review B. 1987, 35:7770.

[62] Le K Q: Finite element analysis of quantum states in layered quantum semiconductor structures with band nonparabolicity effect. Microwave and Optical Technology Letters. 2009, 51:1.

[63] Junique S, Wang Q, Martijn H H, Guo J, Noharet B, Borglind J, Hirschauer B, Malm H, Agren D, Oeberg O, Andersson J Y: Multiple quantum well spatial light modulators: Design, fabrication, characterization. Proceedings of SPIE 4457, Spatial Light Modulators: Technology and Applications, 62.

[64] Sonkar R K, Das U: Fabrication of F-ion implanted quantum well intermixed waveguide grating. Photonics Global Conference. Singapore, Dec, 2012, 1–3.

[65] Choy C H W, Chan K S: Theoretical analysis of diffused quantum-well lasers and optical amplifiers. Selected Topics in IEEE Journal of Quantum Electronics. 2003, 9:698–707.

[66] Sun Y H, Xu L J, Zhang B, Xu Q F, Wang R, Dai N, Wu H Z: Theoretical analysis of optical gain in PbSe/$Pb_{1-x}Sr_xSe$ quantum well lasers. Physica Status Solidi(a). 2009, 206:2606–2612.

[67] Sarkar D, Deyasi A: Calculating Absorption Coefficient of Gaussian Double Quantum Well Structure with Band Nonparabolicity for Photodetector in Microwave Spectra: Foundations and Frontiers in Computer, Communication and Electrical Engineering. 2016, CRC Press. Taylor & Francis Group, London, UK. chapter 47: 225–229.

[68] Chakraborty R, Deyasi A, Paul A, Nayak S: Electronic band structure of quantum cascade laser. Accepted in Springer Proceedings in Physics: Advances in Optical Science and Engineering, 2016 [in press].